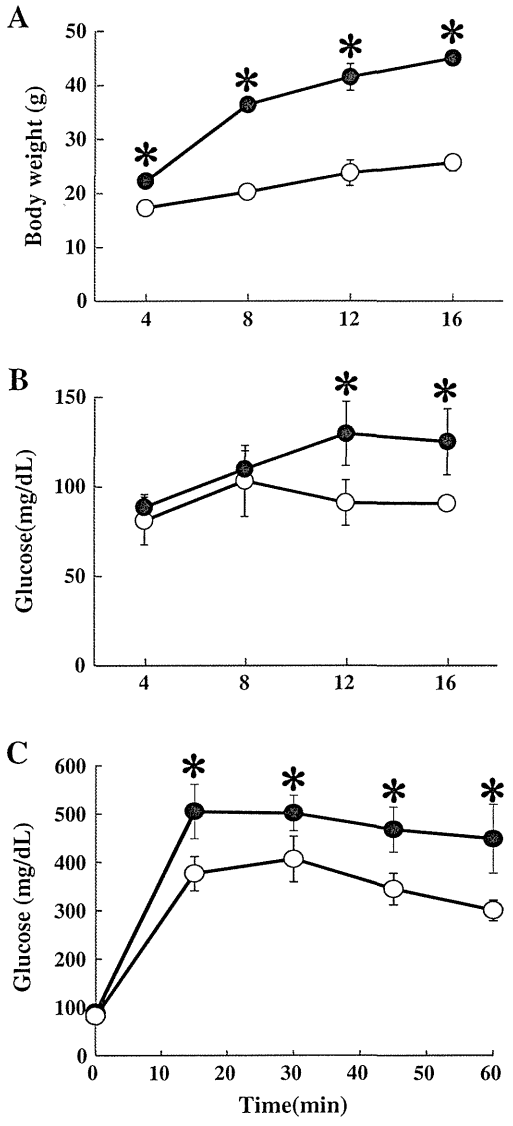

Fig. 1 – Characteristics of KK-A^y mice. Time course changes of body weight (A) and fasting blood glucose (B) in 4–16 weeks old KK-A^y (closed circles) and C57BL/6 mice (open circles). (C) Oral glucose tolerance test in 4-week-old KK-A^y and C57BL/6 mice. Plasma glucose levels at 15, 30, 45 and 60 min after oral glucose administration were measured. C57BL/6 mice are served as control. Each value represents mean ± SD (n = 4 for each group). *, $p < 0.05$ compared with the values of control.

compared to those of age-matched C57BL/6 mice (Fig. 1A) and the glucose concentrations were significantly elevated in 12- and 16-week-old KK-A^y mice compared with those of age-matched C57BL/6 mice (Fig. 1B). OGTT was analyzed at 4 weeks of age (Fig. 1C). The glucose concentrations during the course of glucose loading were significantly higher in 4-week-old KK-A^y mice than in C57BL/6 mice. This result indicates that glucose intolerance was initiated in 4-week-old KK-A^y mice although the fasting glucose concentrations did not show any differences between the 4-week-old KK-A^y mice and C57BL/6 mice. To obtain insights into the molecular differences from the early onset of T2DM, we investigated differential serum proteome analysis between 4-week-old male KK-A^y as T2DM and age-matched male C57BL/6 mice as wild-type mice. In the 2-D LC–MS/MS analysis, a total of 227 unique proteins were identified in the iTRAQ experiments at both the significance threshold $p < 0.05$ and the 5% false discovery rate threshold level (Supplementary Table 1). For the selection of differentially expressed proteins, we selected proteins using the following criteria: (1) the protein quantitation values between the KK-A^y and C57BL/6 groups were significantly different with a p value < 0.05. (2) Proteins detected only in one group were also included as differentially expressed proteins. A total of 45 proteins were selected as differentially expressed proteins. Twenty five proteins among the 45 proteins were found to be up-regulated (Tables 1 and 2), and the other 20 proteins were down-regulated (Tables 3 and 4).

3.2. *Interaction networks and functional pathway analysis*

To gain insights into the biological changes in the KK-A^y versus C57BL/6 mice, the differentially expressed proteins were categorized according to the Gene Ontology (GO) classes "cellular component" and "molecular function". In the cellular component of GO analysis, differentially expressed proteins were located in the extracellular space (64%), membrane attack complex (10%), high-density lipoprotein particle (13%), and plasma lipoprotein particle (13%) (Fig. 2A). According to the molecular functions, most of the differentially expressed proteins were associated with peptidase inhibitor activity (50%), serine hydrolase activity (31%), and lipoprotein binding (19%) (Fig. 2B).

In the IPA analysis, 45 differentially expressed proteins were eligible for network analysis based on the IPA Knowledge Base criteria. IPA generated 3 interaction networks (Supplementary Table 2). Top-rated networks are related to: metabolic disease, endocrine system disorders, and energy production (Fig. 3), and lipid metabolism, molecular transport, and small molecule biochemistry (data not shown). Each network consists of 35 proteins, of which 13 were included in our list, and had a score of 23. Fig. 3 shows that 7 of 13 differentially expressed proteins are modulated directly by peroxisome proliferator activated receptor α, Ppara (p-value of overlap = 3.75×10^{-9}, Supplementary Table 3). Furthermore, 3 of 14 differentially expressed proteins are shown to be modulated directly by nuclear factor, erythroid derived 2, like 2, Nfe2l2 (p-value of overlap = 3.73×10^{-2}, Supplementary Table 3), which also interacted with Ppara.

3.3. *Validation of the selected proteins by MRM analysis*

In the iTRAQ experiments, we analyzed 3 biological replicates per group. This small number of samples could introduce many false positive findings. For the validation of the iTRAQ results, we carried out relative quantification of the identified proteins by MRM analysis using an independent sample set (the sera obtained from 4-week-old KK-A^y and C57BL/6 mice (n = 5/each group)) from that used in the iTRAQ experiments. In this work, proteotyptic peptides were chosen based on iTRAQ results and shotgun proteomic identification data using MRMPilot software. For MRM, 34 of

Table 1 – Increased serum proteins in KK-A^y mice compared to C57BL/6 mice.

Accession number	Entry name	Protein name	Relative protein ratio [a]		KK-A^y: C57BL/6	p-Value
			KK-A^y	C57BL/6		
Q61147	CERU_MOUSE	Ceruloplasmin	1.29 ± 0.07	1.05 ± 0.04	1.23	1.2E−02
P42703	LIFR_MOUSE	Leukemia inhibitory factor receptor	1.05 ± 0.03	0.83 ± 0.09	1.27	3.3E−02
P11589	MUP2_MOUSE	Major urinary protein 2	1.02 ± 0.09	0.8 ± 0.03	1.27	2.9E−02
Q06890	CLUS_MOUSE	Clusterin	1.19 ± 0.06	0.93 ± 0.06	1.28	1.4E−02
P08226	APOE_MOUSE	Apolipoprotein E	1.25 ± 0.16	0.9 ± 0.07	1.38	4.9E−02
Q8K182	CO8A_MOUSE	Complement component C8 alpha chain	1.18 ± 0.03	0.74 ± 0.08	1.59	1.7E−03
P19221	THRB_MOUSE	Prothrombin	1.36 ± 0.05	0.85 ± 0.11	1.60	3.8E−03
P06683	CO9_MOUSE	Complement component C9	1.38 ± 0.12	0.81 ± 0.09	1.69	5.5E−03
P20918	PLMN_MOUSE	Plasminogen	1.03 ± 0.05	0.61 ± 0.04	1.70	9.9E−04
P02762	MUP6_MOUSE	Major urinary protein 6	1.73 ± 0.24	0.74 ± 0.12	2.34	6.6E−03
P07759	SPA3K_MOUSE	Serine protease inhibitor A3K	1.53 ± 0.12	0.60 ± 0.05	2.56	6.0E−04
P09813	APOA2_MOUSE	Apolipoprotein A-II	1.83 ± 0.45	0.64 ± 0.17	2.85	2.6E−02
P04186	CFAB_MOUSE	Complement factor B	1.58 ± 0.09	0.52 ± 0.09	3.05	3.1E−04

[a] The relative protein ratios to an internal standard identified by iTRAQ are used and expressed as mean ± SD.

45 differentially expressed proteins were selected by the criteria described in the Materials and methods. Forty eight peptides representing 34 proteins were selected for MRM analysis. Finally, a total of 102 transitions were used for targeting 34 peptides of 34 proteins. The complete transition list is shown in Supplementary Table 4. For each of the 34 target proteins, three transitions were monitored for each peptide. Supplementary Fig. 2 displays a typical XIC (extracted ion chromatogram) overlay of the predetermined different transitions for the 34 proteins. The XIC peaks of the different transitions for each target protein were detected at the same retention time. Each resulting MRM peak was also examined by full scan MS/MS. The MS/MS spectrum for each MRM peak confirmed the sequence validation of the hypothesized peptide as shown in Supplementary Fig. 3. Individual serum samples were digested and analyzed in duplicate. Among them, 17 proteins showed significant differences between 4-week-old KK-A^y and C57BL/6 mice, which validated the iTRAQ results (Table 5). Retinol-binding protein 4 (RBP4) was found to be increased in 4-week-old KK-A^y mice compared with C57BL/6 mice in the MRM analysis although the expression of RBP4 was decreased in KK-A^y mice in the iTRAQ result. The inconsistency has arisen from the selection of the peptides for the quantitation in the iTRAQ experiments. Relative protein quantitation of RBP4 in C57BL/6 mice was calculated using 4 peptides in the iTRAQ experiments; however, only 2 of the 4 peptides were used for the quantitation in KK-A^y mice samples because other 2 peptides were miscleaved in KK-A^y mice samples. Taken together, we adopted the data obtained from the MRM analysis for the RBP4 protein quantitation. Furthermore, for further analyses of the candidate proteins, the levels of the 34 proteins in the sera of 12-week-old KK-A^y and C57BL/6 mice were also analyzed by MRM analysis because the glucose concentrations in KK-A^y mice were significantly elevated from the age of 12 weeks compared to the C57BL/6 group (Fig. 1B). Eight of the 34 proteins still showed significant differences between 12-week-old KK-A^y and C57BL/6 mice. Among the 8 proteins mentioned above, proteins with a significant increase included 7 proteins: apolipoprotein (apo) A-II, carboxypeptidase N catalytic chain, clusterin, inter-alpha-trypsin inhibitor heavy chain H3, RBP4, serine protease inhibitor A3K (SERPINA3K), and serum amyloid P-component; and another protein with a significant decrease was apo A–I (Table 5).

Table 2 – Identified and quantitated serum proteins only in KK-A^y mice.

Accession number	Entry name	Protein name	Relative protein ratio [a]
Q8BH35	CO8B_MOUSE	Complement component C8 beta chain	1.54 ± 0.10
Q8R121	ZPI_MOUSE	Protein Z-dependent protease inhibitor	1.21 ± 0.07
Q9ET66	PI16_MOUSE	Peptidase inhibitor 16	1.41 ± 0.15
Q9WVJ3	CBPQ_MOUSE	Carboxypeptidase Q	1.05 ± 0.04
Q9JJN5	CBPN_MOUSE	Carboxypeptidase N catalytic chain	1.01 ± 0.16
P31532	SAA4_MOUSE	Serum amyloid A-4 protein	1.43 ± 0.18
P00920	CAH2_MOUSE	Carbonic anhydrase 2	1.33 ± 0.15
P02535	K1C10_MOUSE	Keratin, type I cytoskeletal 10	1.72 ± 0.86
P12246	SAMP_MOUSE	Serum amyloid P-component	1.34 ± 0.20
P52480	KPYM_MOUSE	Pyruvate kinase isozymes M1/M2	1.14 ± 0.16
Q5FW60	MUP20_MOUSE	Major urinary protein 20	3.00 ± 0.75
Q61704	ITIH3_MOUSE	Inter-alpha-trypsin inhibitor heavy chain H3	1.14 ± 0.11

[a] The relative protein ratios to an internal standard identified by iTRAQ are used and expressed as mean ± SD.

3.4. *SERPINA3-induced changes in endothelial cell monolayer permeability*

Among the 8 differentially expressed proteins, SERPINA3K was chosen for further analyses. SERPINA3K was selected on the basis of the possible implications for diabetic retinopathy

Table 3 – Decreased serum proteins in KK-A^y mice compared to C57BL/6 mice.

Accession number	Entry name	Protein name	Relative protein ratio [a]		KK-A^y: C57BL/6	p-Value
			KK-A^y	C57BL/6		
Q00724	RET4_MOUSE	Retinol-binding protein 4	0.71 ± 0.06	1.40 ± 0.25	0.51	2.0E−02
P11859	ANGT_MOUSE	Angiotensinogen	0.73 ± 0.10	1.22 ± 0.19	0.60	3.1E−02
P23953	EST1C_MOUSE	Carboxylesterase 1C	0.62 ± 0.03	1.04 ± 0.06	0.60	9.6E−04
Q60994	ADIPO_MOUSE	Adiponectin	0.68 ± 0.08	1.09 ± 0.13	0.62	1.8E−02
P32261	ANT3_MOUSE	Antithrombin-III	0.75 ± 0.07	1.19 ± 0.05	0.63	1.5E−03
O08677	KNG1_MOUSE	Kininogen-1	0.61 ± 0.04	0.90 ± 0.10	0.67	1.7E−02
Q00623	APOA1_MOUSE	Apolipoprotein A-I	0.98 ± 0.01	1.42 ± 0.06	0.69	4.3E−04
P21614	VTDB_MOUSE	Vitamin D-binding protein	0.84 ± 0.03	1.18 ± 0.01	0.71	7.6E−05
Q8BND5	QSOX1_MOUSE	Sulfhydryl oxidase 1	0.80 ± 0.04	1.08 ± 0.04	0.74	2.9E−03
O89020	AFAM_MOUSE	Afamin	0.88 ± 0.05	1.18 ± 0.02	0.74	1.5E−03
Q61730	IL1AP_MOUSE	Interleukin-1 receptor accessory protein	0.63 ± 0.02	0.84 ± 0.06	0.74	9.8E−03
Q06770	CBG_MOUSE	Corticosteroid-binding globulin	1.38 ± 0.13	1.81 ± 0.12	0.76	2.7E−02
P26262	KLKB1_MOUSE	Plasma kallikrein	0.76 ± 0.07	0.98 ± 0.07	0.78	3.6E−02
Q91X72	HEMO_MOUSE	Hemopexin	0.79 ± 0.10	1.02 ± 0.06	0.78	4.9E−02
Q61129	CFAI_MOUSE	Complement factor I	0.82 ± 0.07	0.98 ± 0.04	0.84	4.4E−02
Q01339	APOH_MOUSE	Beta-2-glycoprotein 1	0.78 ± 0.04	0.91 ± 0.01	0.86	1.5E−02

[a] The relative protein ratios to an internal standard identified by iTRAQ are used and expressed as mean ± SD.

in rat models [19,20]. However, it remains to be elucidated whether human homologue, SERPINA3 is associated with the development of T2DM and/or diabetic retinopathy. Blood-retinal barrier breakdown contributes to macular edema, which occurs in over 25% of people with diabetes and correlated highly with visual impairment in people with diabetic retinopathy [21]. Therefore, we focused on the effects of SERPINA3 on endothelial cell monolayer permeability. To this end, we sought to investigate the impact of SERPINA3 on HRMVECs. Post-confluent serum-starved HRMVECs incubated with SERPINA3 exhibited a dose-dependent increase in endothelial permeability reflected as a decrease in transendothelial electrical resistance, whereas electrical impedance for the untreated HRMVECs was almost unchanged. Fig. 4A is a representative ECIS graph demonstrating the real-time loss of electrical resistance across the HRMVEC monolayer. Permeability increased steadily after SERPINA3 was added, and continued to decline up to 8 h after treatment. Fig. 4B–D is the typical real-time traces of the Rb, α, and Cm in the SERPINA3-treated HRMVECs. After HRMVECs were treated with SERPINA3 (time = 0 in Fig. 4B–D), the cell-to-cell resistances gradually decreased, and the cell-to-extracellular matrix interaction slightly decreased, whereas membrane capacitance was almost unchanged. These results indicate that SERPINA3 treatment mainly caused the decrease of HRMVEC cell-to-cell resistances. Consistent with the ECIS data, we observed that SERPINA3 treatment caused a massive disruption of HRMVEC monolayers (data not shown).

Table 4 – Identified and quantitated serum proteins only in C57BL/6 mice.

Accession number	Entry name	Protein name	Relative protein ratio [a]
P09581	CSF1R_MOUSE	Macrophage colony-stimulating factor 1 receptor	1.23 ± 0.07
Q62351	TFR1_MOUSE	Transferrin receptor protein 1	1.34 ± 0.36
Q8CIF4	BTD_MOUSE	Biotinidase	1.10 ± 0.13
P04939	MUP3_MOUSE	Major urinary protein 3	1.99 ± 0.49

[a] The relative protein ratios to an internal standard identified by iTRAQ are used and expressed as mean ± SD.

3.5. *SERPINA3-induced changes in endothelial cell proliferation and migration*

Proliferation and migratory capability of vascular endothelial cells have a pivotal role in the maintenance of microvascular integrity and angiogenesis. Proliferative capacity of HRMVECs treated with or without SERPINA3 was compared. We found that treatment with SERPINA3 barely affected the proliferative ability in HRMVECs (Fig. 5A).

To assess the effects of SERPINA3 on migratory capability of HRMVECs, an ECIS-based wound-healing assay was performed. We conducted a wounding experiment on single-point ECIS arrays with a single 250 μm-diameter working electrode from which the interrogating electrical current originates, then passes through the monolayer and finally reaches the surrounding counterelectrode. Again, monolayers were found to mature when measured electrically. Post-confluent serum-starved HRMVECs were treated with various doses of SERPINA3 for 6 h, and then monolayers were electrically removed from the central working electrode by driving 1400 μA at 60 kHz through the circuit for 20 s. When assessed 18 h after the SERPINA3 treatment, little differences were observed between the four conditions (Fig. 5B). After completion of the wound closure process, monolayer resistance was found to return to values similar to prewounding levels.

4. Discussion and conclusions

In this paper, we investigated the serum proteome of KK-A^y mice in a pre-diabetic state compared to wild C57BL/6 mice in an attempt to uncover early diagnostic markers of diabetes

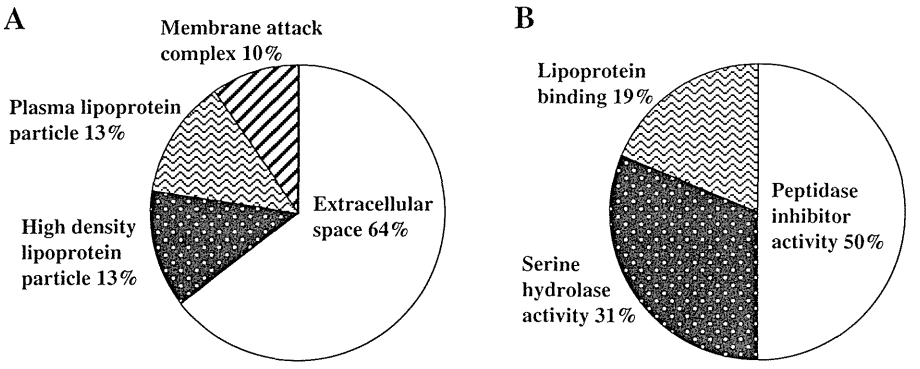

Fig. 2 – Gene ontology terms for cellular components (A), and molecular functions (B) of the differentially expressed proteins between the sera of KK-A^y and C57BL/6 mice.

that are maintained through a diabetic phenotype. We used iTRAQ-based two-dimensional LC–MS/MS serum profiling, and identified several differentially proteins at the pre-diabetic stage. The differential expression was confirmed by MRM analysis, which is fast gaining ground as a sensitive, specific, and cost-effective methodology for relative quantification of candidate proteins. Using these techniques, we have identified eight candidate proteins of interest including SERPINA3K, which may be important in the pathology of T2DM and/or diabetic retinopathy.

Several published studies have reported proteomic alterations in diabetes. During the preparation of this manuscript, Ressom et al. reported a similar approach for a large scale proteomic study aimed at identifying and validating changes

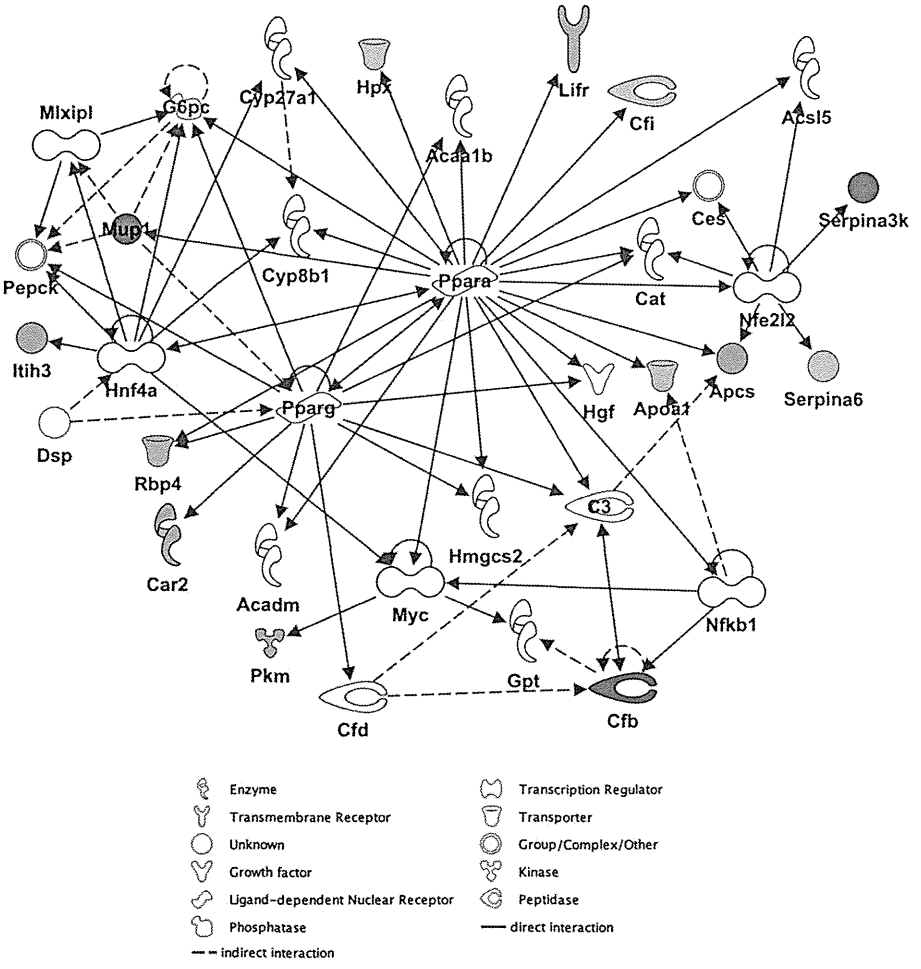

Fig. 3 – Interaction network analysis based on the IPA Knowledge Base criteria. The top-rated network is shown. This network is related to metabolic disease, endocrine system disorders, and energy production. Colored molecules: green; decreased in KK-A^y mice sera, and red; increased in KK-A^y mice sera.

Table 5 – Validation of differentially expressed proteins by MRM assay. Differentially expressed proteins in the iTRAQ experiments were analyzed by MRM assay. The values represent the normalized area under the most intense peak of the target peptides, and are represented as mean ± SD. Duplicate analyses were performed for each of the mouse serum samples.

Accession number	Protein name	Peptide sequence	4-week-old				12-week-old			
			C57BL/6 (B6)	KK-A^y (A^y)	A^y/B6	*p*-Value	C57BL/6 (B6)	KK-A^y (A^y)	A^y/B6	*p*-Value
Q60994	Adiponectin	AVLFTYDQYQEK	1.62 ± 0.71	1.19 ± 0.40	0.74	0.28	1.55 ± 0.69	0.37 ± 0.08	0.24	0.01*
O89020	Afamin	AAPITQYLK	26.36 ± 12.46	22.51 ± 7.73	0.85	0.57	8.41 ± 2.1	9.67 ± 3.20	1.15	0.48
P11859	Angiotensinogen	TLHDQLVLAAEK	2.30 ± 1.01	1.78 ± 0.16	0.78	0.29	0.64 ± 0.27	0.85 ± 0.23	1.32	0.24
P32261	Antithrombin-III	TEDGFSLK	1.38 ± 0.54	0.18 ± 0.25	0.13	2.E−03*	0.62 ± 0.32	0.66 ± 0.32	1.08	0.81
Q00623	Apolipoprotein A-I	TQVQSVIDK	315.84 ± 67.55	0.10 ± 0.11	3.E−04	6.E−06*	84.87 ± 56.38	7.17 ± 5.33	0.08	0.02*
P09813	Apolipoprotein A-II	THEQLTPLVR	60.59 ± 24.63	171.35 ± 63.93	2.83	0.01*	8.07 ± 4.36	60.09 ± 26.56	7.45	3.E−03*
P08226	Apolipoprotein E	LQAEIFQAR	28.41 ± 13.60	37.81 ± 14.93	1.33	0.33	3.63 ± 1.1	15.66 ± 4.37	4.32	3.E−04*
Q01339	Beta-2-glycoprotein 1	YTSFEYPK	36.76 ± 12.77	24.30 ± 18.78	0.66	0.25	17.04 ± 4.23	23.48 ± 4.21	1.38	0.04*
Q8CIF4	Biotinidase	GLSSGLVTAALYGR	0.24 ± 0.06	0.23 ± 0.09	0.96	0.85	0.11 ± 0.08	0.11 ± 0.03	0.97	0.92
P23953	Carboxylesterase 1C	EGASEEETNLSK	10.65 ± 6.01	6.62 ± 5.93	0.62	0.32	1.09 ± 0.59	3.90 ± 4.75	3.57	0.23
Q9JJN5	Carboxypeptidase N catalytic chain	AVIQWIR	0.79 ± 0.27	1.20 ± 0.26	1.52	0.04*	0.39 ± 0.28	0.74 ± 0.16	1.92	0.04*
Q61147	Ceruloplasmin	AGLQAFFQVR	5.46 ± 4.68	12.49 ± 2.27	2.29	0.02*	1.19 ± 1.1	2.23 ± 1.36	1.87	0.22
Q06890	Clusterin	ASGIIDTLFQDR	2.48 ± 0.64	4.28 ± 0.79	1.57	0.02*	1.26 ± 0.38	2.58 ± 0.12	2.24	4.E−05*
Q8K182	Complement component C8 alpha chain	TEGTTVDEVQK	0.09 ± 0.04	0.05 ± 0.05	0.61	0.25	0.02 ± 0.02	0.06 ± 0.06	2.37	0.27
Q8BH35	Complement component C8 beta chain	ALEEFQSEVSSC[CAM]R	0.21 ± 0.10	0.99 ± 0.64	4.78	0.03*	0.08 ± 0.02	0.42 ± 0.65	5.32	0.28
P06683	Complement component C9	AVEDYIDEFSTK	0.13 ± 0.05	1.43 ± 0.67	11.07	3.E−03*	0.13 ± 0.15	0.19 ± 0.07	1.42	0.48
Q06770	Corticosteroid-binding globulin	AGEQINNHVK	0.08 ± 0.04	0.07 ± 0.05	0.91	0.82	0.10 ± 0.07	0.08 ± 0.05	0.80	0.59
Q91X72	Hemopexin	LYVSSGR	124.18 ± 37.50	98.01 ± 27.86	0.79	0.25	109.93 ± 37.67	126.32 ± 33.71	1.15	0.49
Q61704	Inter-alpha-trypsin inhibitor heavy chain H3	SLPEGVVDGIEVYSTK	0.21 ± 0.18	5.25 ± 2.72	25.18	3.E−03*	0.10 ± 0.05	0.30 ± 0.11	3.11	0.01*
O08677	Kininogen-1	QFNPGVK	11.81 ± 4.26	8.73 ± 3.31	0.74	0.24	8.84 ± 4.79	8.30 ± 3.43	0.94	0.84
P42703	Leukemia inhibitory factor receptor	ITGLVGPR	3.08 ± 0.87	8.78 ± 1.83	2.85	2.E−04*	2.7 ± 1.38	1.61 ± 0.37	0.60	0.12
P09581	Macrophage colony-stimulating factor 1 receptor	ESTSTGIWLK	1.02 ± 0.36	0.55 ± 0.25	0.54	0.04*	0.47 ± 0.24	0.35 ± 0.10	0.73	0.31
P04939	Major urinary protein 3	ENIIDLTNVNR	2.65 ± 0.65	2.89 ± 0.63	1.09	0.58	2.31 ± 1.1	1.52 ± 0.25	1.22	0.55
Q9ET66	Peptidase inhibitor 16	AESPEAEAESPLSSEALVPVLPAQER	0.03 ± 0.01	0.05 ± 0.01	2.10	4.E−03*	0.02 ± 0.01	0.01 ± 3E−03	0.56	0.07
P26262	Plasma kallikrein	SADNLVSGFSLK	1.09 ± 0.85	0.77 ± 0.47	0.71	0.49	0.09 ± 0.04	0.15 ± 0.08	1.66	0.15
P20918	Plasminogen	TGIGNGYR	0.16 ± 0.07	0.58 ± 0.34	3.69	0.03*	0.11 ± 0.06	0.18 ± 0.08	1.60	0.17
Q8R121	Protein Z-dependent protease inhibitor	LILVDYVLFK	0.17 ± 0.07	0.39 ± 0.18	2.33	0.04*	0.57 ± 0.28	0.54 ± 0.47	0.95	0.91
P19221	Prothrombin	DNLSPPLGQC[CAM]LTER	1.62 ± 1.41	2.21 ± 1.62	1.36	0.56	0.25 ± 0.14	1.04 ± 0.38	4.19	2.E−03*
P52480	Pyruvate kinase isozymes M1/M2	LDIDSAPITAR	0.11 ± 0.06	0.44 ± 0.31	4.19	0.04*	0.07 ± 0.04	0.06 ± 0.03	0.85	0.59
Q00724	Retinol-binding protein 4	LQNLDGTC[CAM]ADSYSFVFSR	0.39 ± 0.17	0.79 ± 0.20	2.01	0.01*	0.05 ± 0.03	0.11 ± 0.03	2.26	0.01*
P07759	Serine protease inhibitor A3K	TLFPSQIEELNLPK	0.39 ± 0.18	68.06 ± 28.55	176.70	7.E−04*	1.23 ± 2.06	9.28 ± 2.16	7.54	3.E−04*
P12246	Serum amyloid P-component	SQSLFSYSVK	0.13 ± 0.14	1.52 ± 0.44	11.59	2.E−04*	2E−03 ± 9E−04	0.21 ± 0.17	85.66	0.04*
Q8BND5	Sulfhydryl oxidase 1	SYVQFFFGC[CAM]R	0.30 ± 0.20	0.22 ± 0.14	0.73	0.48	0.07 ± 0.02	0.09 ± 0.03	1.19	0.42
P21614	Vitamin D-binding protein	TQVPEVFLSK	101.77 ± 35.17	88.03 ± 19.21	0.87	0.47	54.49 ± 21.66	70.01 ± 17.57	1.28	0.25

* $p < 0.05$ to age-matched C57BL/6 mice.

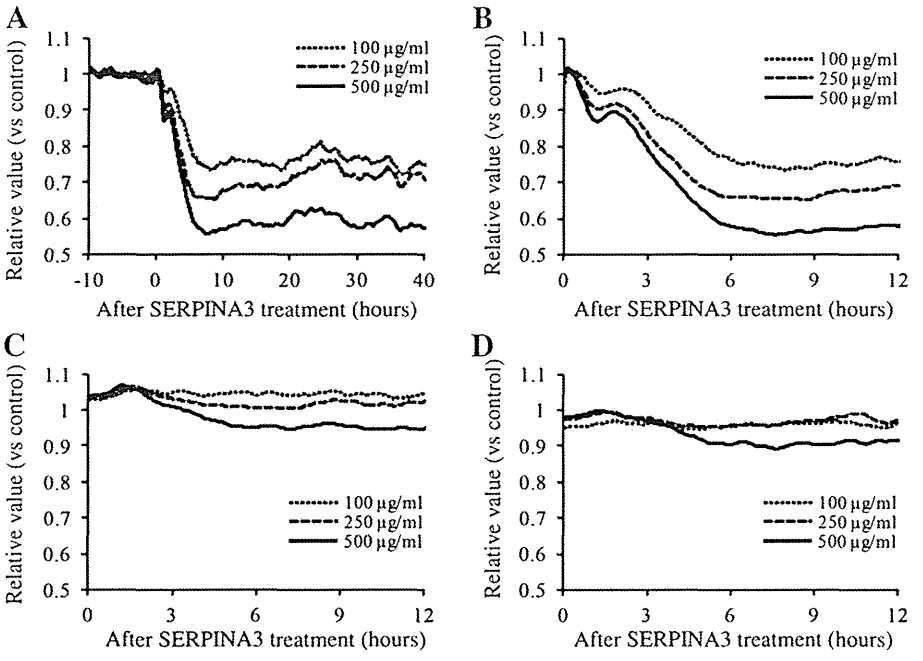

Fig. 4 – Monolayer barrier function of human retinal microvascular endothelial cells (HRMVECs) was notably decreased by SERPINA3 treatment. Post-confluent serum-starved HRMVECs were treated with SERPINA3 (100, 250, and 500 μg/ml) for 40 h. HRMVECs treated without SERPINA3 were used as control. (A) Impedance measurements at 16 kHz were obtained from HRMVECs treated with SERPINA3. (B–D) ECIS Zθ measurements were modeled to obtain the Rb (modeled barrier function, B), α (modeled cell-to-extracellular matrix interactions, C), and Cm (modeled membrane capacitance, D). Each trace of the impedance, Rb, α, and Cm is shown as an average of three replicate wells and representative of three independent experiments. Each value was normalized to the control.

in protein abundance among human serum obtained from a cohort of nondiabetic control subjects and patients diagnosed with T2DM [22]. The study reported here uses a similar approach nevertheless we analyzed the serum proteome analysis using T2DM mice model. However, it is novel in terms of quantitative profiling and comprehensive validation of the target proteins in individual samples. A limitation of this study is the use of T2DM mouse with obesity. We cannot delineate the differential markers of obesity and T2DM. Consequently, further validation analyses are required using human healthy and T2DM serum samples, which are now under investigation.

Among the eight serum proteins validated by MRM analysis, several published studies have also reported the differential expression of apo-AI, apo-AII, carboxypeptidase N catalytic chain, clusterin, inter-alpha-trypsin inhibitor heavy chain H3, SERPINA3K, and serum amyloid P-component in patients with diabetes and/or microvasculopathy [22–24]. Identification of RBP4 has not been reported in iTRAQ-based serum proteomic analysis, however, elevated levels of RBP4 have been reported in patients with obesity and metabolic syndrome [25–27]. The levels of RBP4 seem to be regulated in visceral adipose tissue. In the current study, SERPINA3K was chosen for further analyses because it remains to be elucidated whether human homologue, SERPINA3 is associated with the development of T2DM and/or diabetic retinopathy.

SERPINA3K was originally identified as a SERPIN family member with specific inhibitory effect on tissue kallikrein [28]. It is expressed in the liver, kidney, pancreas, and retina [29,30]. The previous studies have shown decreased retinal levels of SERPINA3K in a diabetic retinopathy rat model [19]. SERPINA3K attenuates inflammation in the retina with retinopathy [31] and has been found to inhibit ischemia-induced retinal neovascularization [20]. Recently, Zhang et al. have reported that rat SERPINA3K inhibited angiogenesis through Wnt/β-catenin signaling pathway as LRP6 antagonist [32]. In the present study, we found that SERPINA3K was consistently induced in KK-A^y mice sera compared with C57BL/6 mice. We also investigated the potential association between human SERPINA3 levels and T2DM. The serum SERPINA3 levels were approximately 180 μg/mL in healthy subjects, and the serum SERPINA3 levels were higher in T2DM and diabetic retinopathy patients compared to those in healthy control subjects (data not shown). In the IPA network analysis, SERPINA3 is shown to be modulated directly by Nfe2l2 (Fig. 2) [33]. Nfe2l2, also known as nuclear factor E2-related factor 2 (Nrf2) is a transcription factor that functions as a master regulator of the cellular adaptive response to oxidative stress [34]. Hyperglycemia is the metabolic hallmark of diabetes and leads to widespread cellular damage through oxidative stress. Recently, Slitt et al. reported that enhanced Nrf2 activation inhibited lipid accumulation in white adipose tissue, suppressed adipogenesis, induced insulin resistance and glucose intolerance, and increased hepatic steatosis in diabetic $Lep^{ob/ob}$ mice [35]. We analyzed the tissue distribution of SERPINA3 in KK-A^y mice and found that SERPINA3 is highly expressed in liver and also detected in pancreas, white adipose tissue, skeletal muscle, kidney, and heart (data not shown). We

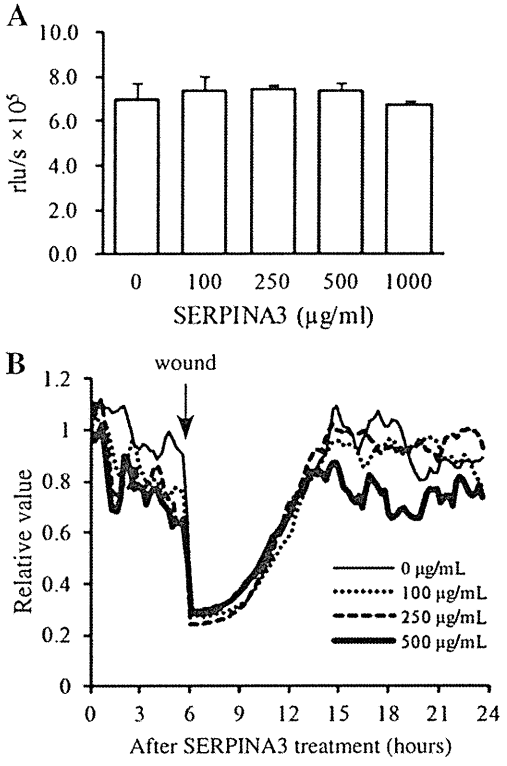

Fig. 5 – SERPINA3 did not significantly affect the proliferative ability or migratory capability of HRMVECs. (A) BrdU incorporation in HRMVECs. The cells were treated with or without SERPINA3 (100, 250, 500, 1000 μg/mL) and labeled with BrdU from 18 to 24 h after treatment. Data are expressed as mean ± SD values of triplicate samples. (B) Electrical wound-healing assay by ECIS Zθ. Post-confluent serum-starved HRMVECs were treated with SERPINA3 for 6 h, after which an elevated voltage pulse was applied to the electrode (marked with an arrow). Impedance values were normalized by dividing the values by those measured just prior to the addition of SERPINA3 (at time = 0).

speculate that enhanced activation of Nrf2 in liver may cause the increase in serum SERPINA3 from the early onset of T2DM although further studies are required to identify the precise mechanisms.

To gain insights into the function of SERPINA3, we assessed the effects of SERPINA3 on endothelial cell monolayer permeability. An ECIS assay was carried out by varying SERPINA3 concentrations ranging from 100 to 500 μg/mL, which cover the physiological concentration range in healthy subjects and T2DM patients. An *in vitro* assay revealed that SERPINA3 increased transendothelial permeability of HRMVECs (Fig. 5). Diabetic maculopathy, a leading cause of vision loss in patients with T2DM is characterized by hyperpermeability of retinal blood vessels with subsequent formation of macular edema and hard exudates. Epidemiological studies have suggested that glycemic control plays a major role in the development of vascular complications of diabetes [36]. SERPINA3 may become a downstream glycemic target that contributes to increased retinal vascular permeability that could be targeted therapeutically, and a blood biomarker of diabetic retinopathy although further investigations are required. In addition, our present study showed that SERPINA3 showed little proliferative ability and little effect of migratory capability of HRMVECs, which is inconsistent with the previous reports [20,32]. The discrepancy may have risen from interspecies differences. Rat SERPINA3K shares high degree of sequence identity with mouse SERPINA3K (70–71%) and human SERPINA3 (50–55%). However, mouse SERPINA3K and human SERPINA3 are known to be induced by acute inflammation in contrast to rat SERPINA3K which is a negative acute-phase protein [37]. Further studies are necessary to clarify the precise mechanism of action of SERPINA3 for cell proliferation.

In the current study, 11 of 45 differentially expressed proteins could not be validated by MRM analysis using an independent sample set. In MRM, there are several possible reasons why not all targeted proteins were detected. They include 1) the absence of appropriate peptide regions of the targeted proteins which meet the criteria described in the Materials and methods, and 2) the MS peak of the target protein was hard to be detected due to high background noise. For the validation of the 11 candidate proteins, we need to analyze the serum levels by other methods such as ELISA or Western blotting. We now investigate the potential association between the levels of the 11 candidate proteins and T2DM using human healthy and T2DM serum samples. We would examine the functional properties of the validated proteins including the 7 MRM-validated proteins in the future studies.

In summary, iTRAQ and MRM based discovery-through-verification strategy led to the identification of several differentially protein including SERPINA3K in T2DM. With the identified expressed proteins, our proteomics study could provide valuable clues to better understand the underlying mechanisms associated with T2DM.

Supplementary data to this article can be found online at http://dx.doi.org/10.1016/j.jprot.2013.03.014.

Conflict of interest

The authors report no conflict of interest.

Acknowledgments

We thank W. Iwata, T. Okamura, M. Goto and the technical staff of the Division of Animal Models at the National Center for Global Health and Medicine for their technical assistances. This work was supported by a Grant-in-Aid (Research on Biological Markers for New Drug Development, H20-009) from the Ministry of Health, Labor, and Welfare of Japan, a Grant-in-Aid for Scientific Research (KAKENHI, 23500870) from the Ministry of Education, Culture, Sports, Science and Technology of Japan, and a grant from the National Center for Global Health and Medicine (23S104).

REFERENCES

[1] Korc M. Diabetes mellitus in the era of proteomics. Mol Cell Proteomics 2003;2:399–404.

[2] Gerich JE. The genetic basis of type 2 diabetes mellitus: impaired insulin secretion versus impaired insulin sensitivity. Endocr Rev 1998;19:491–503.
[3] Klein R, Klein BEK, Moss SE, Cruickshanks KJ. The Wisconsin epidemiologic study of diabetic retinopathy: XVII. The 14-year incidence and progression of diabetic retinopathy and associated risk factors in type 1 diabetes. Ophthalmology 1998;105:1801–15.
[4] Horikawa Y, Yamasaki T, Nakajima H, Shingu R, Yoshiuchi I, Miyagawa J, et al. Identification of a novel variant in the phosphoenolpyruvate carboxykinase gene promoter in Japanese patients with type 2 diabetes. Horm Metab Res 2003;35:308–12.
[5] Vendrell J, Fernandez-Real JM, Gutierrez C, Zamora A, Simon I, Bardaji A, et al. A polymorphism in the promoter of the tumor necrosis factor-α gene (-308) is associated with coronary heart disease in type 2 diabetic patients. Atherosclerosis 2003;167:257–64.
[6] Lindgren CM, Widen E, Tuomi T, Li H, Almgren P, Kanninen T, et al. Contribution of known and unknown susceptibility genes to early-onset diabetes in Scandinavia: evidence for heterogeneity. Diabetes 2002;51:1609–17.
[7] Rao AA, Sridhar GR, Das UN. Elevated butyrylcholinesterase and acetylcholinesterase may predict the development of type 2 diabetes mellitus and Alzheimer's disease. Med Hypotheses 2007;69:1272–6.
[8] Rao AA, Sridhar GR, Srinivas B, Das UN. Bioinformatics analysis of functional protein sequences reveals a role for brain-derived neurotrophic factor in obesity and type 2 diabetes mellitus. Med Hypotheses 2008;70:424–9.
[9] On YK, Park HK, Hyon MS, Jeon ES. Serum resistin as a biological marker for coronary artery disease and restenosis in type 2 diabetic patients. Circ J 2007;71:868–73.
[10] Zhang R, Barker L, Pinchev D, Marshall J, Rasamoelisolo M, Smith C, et al. Mining biomarkers in human sera using proteomic tools. Proteomics 2004;4:244–56.
[11] Dayal B, Ertel NH. ProteinChip technology: a new and facile method for the identification and measurement of high-density lipoproteins apoA-I and apoA-II and their glycosylated products in patients with diabetes and cardiovascular disease. J Proteome Res 2002;1:375–80.
[12] Sundsten T, Eberhardson M, Goransson M, Bergsten P. The use of proteomics in identifying differentially expressed serum proteins in humans with type 2 diabetes. Proteome Sci 2006;4:22.
[13] Suto J, Matsuura S, Imamura K, Yamanaka H, Sekikawa K. Genetics of obesity in KK mouse and effects of A^y allele on quantitative regulation. Mamm Genome 1998;9:506–10.
[14] Unoki-Kubota H, Yamagishi S, Takeuchi M, Bujo H, Saito Y. Pyridoxamine, an inhibitor of advanced glycation end product (AGE) formation ameliorates insulin resistance in obese, type 2 diabetic mice. Protein Pept Lett 2010;17:1177–81.
[15] Huang da W, Sherman BT, Lempicki RA. Systematic and integrative analysis of large gene lists using DAVID bioinformatics resources. Nat Protoc 2009;4:44–57.
[16] Okumura A, Ohta H, Inoue Y, Enami I. Identification of functional domains of the extrinsic 12 kDa protein in red algal PSII by limited proteolysis and directed mutagenesis. Plant Cell Physiol 2001;42:1331–7.
[17] Giaever I, Keese CR. Micromotion of mammalian cells measured electrically. Proc Natl Acad Sci U S A 1991;88:7896–900.
[18] Nishimura M. Breeding of mice strains for diabetes mellitus. Exp Anim 1969;18:147–57.
[19] Hatcher HC, Ma JX, Chao J, Chao L, Ottlecz A. Kallikrein-binding protein levels are reduced in the retinas of streptozotocin-induced diabetic rats. Invest Ophthalmol Vis Sci 1997;38:658–64.
[20] Gao G, Shao C, Zhang SX, Dudley A, Fant J, Ma J-X. Kallikrein-binding protein inhibits retinal neovascularization and decreases vascular leakage. Diabetologia 2003;46:689–98.
[21] Klein R, Klein BEK, Moss SE, Cruickshanks KJ. The Wisconsin epidemiologic study of diabetic retinopathy. Opthalmology 1995;102:7–16.
[22] Kaur P, Rizk NM, Ibrahim S, Younes N, Uppal A, Dennis K, et al. iTRAQ-based quantitative protein expression profiling and MRM verification of markers in type 2 diabetes. J Proteome Res 2012;11:5527–39.
[23] Overgaard AJ, Thingholm TE, Larsen MR, Tarnow L, Rossing P, McGuire JN, et al. Quantitative iTRAQ-based proteomic identification of candidate biomarkers for diabetic nephropathy in plasma of type 1 diabetic patients. Clin Proteomics 2010;6:105–14.
[24] García-Ramírez M, Canals F, Hernández C, Colomé N, Ferrer C, Carrasco E, et al. Proteomic analysis of human vitreous fluid by fluorescence based difference gel electrophoresis (DIGE): a new strategy for identifying potential candidates in the pathogenesis of proliferative diabetic retinopathy. Diabetologia 2007;50:1294–303.
[25] Klöting N, Graham TE, Berndt J, Kralisch S, Kovacs P, Wason CJ, et al. Serum retinol-binding protein is more highly expressed in visceral than in subcutaneous adipose tissue and is a marker of intra-abdominal fat mass. Cell Metab 2007;6:79–87.
[26] Fernández-Real JM, Moreno JM, Ricart W. Circulating retinol-binding protein-4 concentration might reflect insulin resistance-associated iron overload. Diabetes 2008;57:1918–25.
[27] Raila J, Henze A, Spranger J, Möhlig M, Pfeiffer AF, Schweigert FJ. Microalbuminuria is a major determinant of elevated plasma retinol-binding protein 4 in type 2 diabetic patients. Kidney Int 2007;72:505–11.
[28] Chao J, Chai KX, Chen LM, Xiong W, Chao S, Woodley-Miller C, et al. Tissue kallikrein-binding protein is a SERPIN. I. Purification, characterization, and distribution in normotensive and spontaneously hypertensive rats. J Biol Chem 1990;265:16394–401.
[29] Chao J, Tillman DM, Wang MY, Margolius HS, Chao L. Identification of a new tissue-kallikrein-binding protein. Biochem J 1986;239:325–31.
[30] Gettins PG. SERPIN structure, mechanism, and function. Chem Rev 2002;102:4751–803.
[31] Zhang B, Hu Y, Ma JX. Anti-inflammatory and antioxidant effects of SERPINA3K in the retina. Invest Ophthalmol Vis Sci 2009;50:3943–52.
[32] Zhang B, Abreu JG, Zhou K, Chen Y, Hu Y, Zhou T, et al. Blocking the Wnt pathway, a unifying mechanism for an angiogenic inhibitor in the serine proteinase inhibitor family. Proc Natl Acad Sci U S A 2010;107:6900–5.
[33] Kwak MK, Wakabayashi N, Itoh K, Motohashi H, Yamamoto M, Kensler TW. Modulation of gene expression by cancer chemopreventive dithiolethiones through the Keap1-Nrf2 pathway: identification of novel gene clusters for cell survival. J Biol Chem 2003;278:8135–45.
[34] Ishii T, Itoh K, Ruiz E, Leake DS, Unoki H, Yamamoto M, et al. Role of Nrf2 in the regulation of CD36 and stress protein expression in murine macrophages: activation by oxidatively modified LDL and 4-hydroxynonenal. Circ Res 2004;94:609–16.
[35] Xu J, Kulkarni SR, Donepudi AC, More VR, Slitt AL. Enhanced Nrf2 activity worsens insulin resistance, impairs lipid accumulation in adipose tissue, and increases hepatic steatosis in leptin-deficient mice. Diabetes 2012;61:3208–18.
[36] American Diabetes Association. Implications of the diabetes control and complications trial. American Diabetes Association. Diabetes 1993;42:1555–8.
[37] Ohkubo K, Ogata S, Misumi Y, Takami N, Ikehara Y. Molecular cloning and characterization of rat contrapsin-like protease inhibitor and related proteins. J Biochem 1991;109:243–50.

FEBS Letters 587 (2013) 404–409

ELSEVIER

FEBS Letters

journal homepage: www.FEBSLetters.org

Leukocyte cell-derived chemotaxin 2 is a zinc-binding protein

Akinori Okumura [a,1], Takehiro Suzuki [b], Hideyuki Miyatake [b], Tomoya Okabe [c], Yuki Hashimoto [c], Takuya Miyakawa [d], Hai Zheng [d], Hiroyuki Unoki-Kubota [a], Hideaki Ohno [c], Naoshi Dohmae [b], Yasushi Kaburagi [a], Yoshitsugu Miyazaki [c], Masaru Tanokura [d], Satoshi Yamagoe [c,*,1]

[a] Department of Diabetic Complications, Diabetes Research Center, Research Institute, National Center for Global Health and Medicine, Tokyo 162-8655, Japan
[b] Biomolecular Characterization Team, RIKEN, Saitama 351-0198, Japan
[c] Department of Chemotherapy and Mycosis, National Institute of Infectious Diseases, Tokyo 162-8640, Japan
[d] Department of Applied Biological Chemistry, Graduate School of Agricultural and Life Sciences, The University of Tokyo, Tokyo 113-8657, Japan

ARTICLE INFO

Article history:
Received 5 September 2012
Revised 8 December 2012
Accepted 9 January 2013
Available online 22 January 2013

Edited by Christian Griesinger

Keywords:
Leukocyte cell-derived chemotaxin 2
Zinc-binding protein
Electrospray ionization mass spectrometry
X-ray absorption fine structure
Disulfide bond
Oligomerization

ABSTRACT

Leukocyte cell-derived chemotaxin 2 (LECT2) is a secreted hepatic protein that has been associated with several physiological activities. LECT2 belongs to the peptidase M23 family, suggesting that it is a zinc-binding protein. To test this possibility, electrospray ionization mass spectrometry and X-ray absorption fine-structure analysis were performed. Results of these experiments indicated that recombinant mouse LECT2 produced by an animal cell line contains a zinc atom. Furthermore, the recombinant LECT2 was found to be self-oligomerized by disulfide bonds in vitro, but this was suppressed by addition of zinc. These results indicated that zinc stabilizes the LECT2 structure.

Structured summary of protein interactions:
LECT2 and **LECT2** bind by cross-linking study (View interaction)
LECT2 and **LECT2** bind by comigration in gel electrophoresis (View interaction)
LECT2 and **LECT2** bind by comigration in gel electrophoresis (View interaction: 1, 2, 3)
LECT2 and **LECT2** bind by cross-linking study (View interaction: 1, 2, 3)
LECT2 and **LECT2** bind by comigration in gel electrophoresis (View interaction: 1, 2, 3)

1. Introduction

Leukocyte cell-derived chemotaxin 2 (LECT2) has been identified as a human neutrophil chemotactic protein [1]. LECT2 is a secreted hepatic protein with a molecular mass of approximately 16 kDa [2], and the mammalian form has three disulfide bonds [3]. The protein-sequence has been well conserved throughout evolution. Although accumulating evidence indicates that LECT2 is associated with several physiologic functions, their mechanisms are not yet clear [4–9].

LECT2 belongs to the peptidase M23 structural family (PF01551), as described in the pfam data base (http://pfam.sanger.ac.uk), which indicates it is a metalloprotease having a zinc ion as a cofactor. Actually, many proteins of the M23 family have a zinc ion in their catalytic domain that contributes to their protease activity. This protein family is widespread in bacteria, but LECT2 is the only vertebrate protein in the M23 family. It is unclear whether LECT2 has a protease activity.

In this report, the results of electrospray ionization mass spectrometry (ESI-MS) and X-ray absorption fine-structure (XAFS) analysis indicate that recombinant mouse LECT2 produced by a mammalian cell line contains a zinc atom. Furthermore, human and mouse recombinant LECT2 proteins produced by an animal cell line were found to be oligomerized by disulfide linkages in vitro. This oligomerization was accelerated by the presence of EDTA or EGTA and was inhibited by the presence of zinc ions. These results indicate that LECT2 is a zinc-binding protein and that zinc contributes to the stability of the protein structure. They also suggest that zinc plays a crucial role in the biological function of LECT2. Moreover, LECT2 has recently been reported as an amyloid protein [10,11], suggesting that the oligomerization of LECT2 observed in this study might be related to amyloid fibril formation.

2. Materials and methods

2.1. The purification of recombinant mouse LECT2 protein

Recombinant mouse LECT2 (GenBank accession number: BAA33383) was purified using a procedure slightly modified from the original [3]. A stable clone (clone No. 10G) of Chinese hamster

Abbreviation: LECT2, leukocyte cell-derived chemotaxin 2

* Corresponding author. Fax: +81 3 5285 1150.
E-mail address: syamagoe@nih.go.jp (S. Yamagoe).

[1] These authors contributed equally to this work.

0014-5793/$36.00 © 2013 Federation of European Biochemical Societies. Published by Elsevier B.V. All rights reserved.
http://dx.doi.org/10.1016/j.febslet.2013.01.025

ovary (CHO) cells transfected with an expression vector having mouse LECT2 cDNA was grown in Dulbecco's modified Eagle's medium with 5% fetal bovine serum. Five liters of culture medium were harvested and diluted with an equal volume of Milli-Q water. CM-Sepharose fast flow resin (GE Healthcare, Little Chalfont, UK), pre-equilibrated with 50 mM Tris–HCl pH 7.5 (buffer A), was added to the culture fluid (30 ml resin) and stirred for 16 h at 4 °C. The resin was collected by filtration with aspiration over a Kiriyama-rohto (95 mm in diameter, filter paper No. 5B; Kiriyama, Tokyo, Japan), washed exhaustively with buffer A, and eluted with buffer A supplemented with 0.5 M NaCl. The eluent was dialyzed against buffer A overnight, and then loaded onto a Toyopearl DEAE-650 M column (Tosoh, Tokyo, Japan) equilibrated with buffer A. The pass-through fraction was recovered and applied again to the Toyopearl CM-650 M column (Tosoh, Tokyo, Japan) equilibrated with buffer A. After the CM column was washed with buffer A, the proteins were eluted with a 0–0.7 M NaCl linear gradient in buffer A. LECT2-containing fractions were identified using an ELISA [5]. The fractions containing an appreciable amount of mouse LECT2 were pooled and dialyzed against 50 mM Tris–HCl pH 7.5 containing 10% glycerol (buffer B). The dialysate was loaded onto a Mono-S HR 5/5 column (GE Healthcare, Little Chalfont, UK) equilibrated with buffer B and washed with buffer B containing 0.1 M NaCl. Elution was then carried out with a linear gradient of 0.1–0.5 M NaCl in buffer B. The fractions showing a single band on SDS–PAGE by silver staining were pooled and dialyzed against 40 mM HEPES-NaOH pH 7.4, 10% glycerol, 100 mM NaCl. Recombinant human LECT2 was also purified from the culture fluid of an established CHO cell line (clone name C1D8) as described previously [3,12].

2.2. Electrospray ionization mass spectrometry (ESI-MS)

ESI-MS experiments were performed on a Thermo Finnigan LCQ Deca XP plus ion trap mass spectrometer (Thermo Scientific, Waltham, MA, USA) equipped with a handmade nanospray tip (0.1 × 50 mm). For the measurements under acidic and neutral conditions, the ESI-MS spectra were acquired in positive ion mode at a flow rate of 1 μl/min with running solution consisting of 0.075% formic acid (pH 2.6) and 10 mM ammonium formate (pH 6.4), respectively. Recombinant mouse LECT2 was exchanged into the same solution. Electrospray mass spectra were processed using the Biomass convolution and deconvolution algorithms in the Bioworks 3.1 software package (Thermo Scientific).

2.3. X-ray absorption fine structure (XAFS)

Recombinant mouse LECT2 and a recombinant lysostaphin of *Staphylococcus simulans* (Wako, Osaka, Japan) were dialyzed against water prior to analysis. Each protein solution (100 μM) was picked up with Litholoop (ϕ = 0.3 mm) and then was flash-frozen under a cryo-nitrogen stream at 100 K. The frozen samples were shipped to SPring-8 BL26B2 for mail-in data collection [13]. The fluorescence XAFS spectra of these proteins were measured automatically by the SPring-8 Precise Automatic Cryo-sample Exchanger (SPACE) [14,15] in the energy range from 1.290000 to 1.276000 Å with an interval of 0.0001 Å for an exposure time of 3 s with a Si-PIN photodiode detector [16]. The XAFS spectra were analyzed using the software D-Cha (database for crystallography with home-lab arrangement) [13] to assign the wavelengths corresponding to the peak and edge.

2.4. Analysis of LECT2 oligomerization in vitro

Twenty microliters of reaction buffer C (100 mM Tris–HCl pH 7.5, 150 mM NaCl) containing recombinant mouse LECT2 (1 μg) were incubated at 37 °C. To assess the role of divalent ions, we included 5 mM of each reagent (EDTA, EGTA, $ZnCl_2$, $MgCl_2$, $CaCl_2$) in the reaction solution. The reaction was stopped by adding an equal volume of SDS–PAGE sample buffer (250 mM Tris–HCl pH 6.8, 10% lithium dodecyl sulfate, 20% glycerol, 0.04% bromophenol blue) and incubating for 1 h at room temperature. The protein samples (2–8 μl) were subjected to SDS–PAGE on a 5–20% gradient polyacrylamide gel and Western blotting using an anti-mouse LECT2 polyclonal antibody [12]. To examine the reversibility of the zinc ion binding to LECT2, we prepared an EDTA-free solution and two EDTA-containing solutions. Forty microliters of buffer C containing 2 μg of recombinant mouse LECT2 were incubated in the presence or absence of 5 mM EDTA for 6 h at 4 °C. Subsequently, the ETDA-free solution was dialyzed using an Xpress micro Dialyze Cartridge 3.5 kDa (Scienova GmbH, Jena, Germany) against 2 ml of buffer C for 12 h as a control. Each of the EDTA-containing solutions was dialyzed using the same cartridge against buffer C (2 ml) with or without 5 mM $ZnCl_2$ for 12 h at 4 °C. The three dialyzed solutions were then separately re-dialyzed three times against 2 ml of buffer C for 12 h at 4 °C. Finally, these solutions were incubated for 24 h at 37 °C and were subjected to SDS–PAGE and Western blot analysis. All SDS–PAGE were carried out under non-reducing conditions (without DTT treatment and boiling) except when indicated specifically.

3. Results

3.1. Recombinant mammalian LECT2 contains a zinc atom

LECT2 is a member of the peptidase M23 structural family (PF01551 in the pfam data base), indicating it is a metalloprotease containing a zinc ion as a cofactor. Therefore, we first attempted to determine whether LECT2 contains a zinc atom. EMI-MS is an appropriate technique with which to analyze peptide–metal interactions [17]. We used the same preparation of the recombinant mouse LECT2 that was analyzed previously using matrix-assisted laser desorption/ionization time-of-flight mass spectrometry [3], which had indicated the only covalent modification was the presence of three disulfide bonds. Fig. 1 shows typical ESI-MS spectra of the recombinant mouse LECT2 under acidic and neutral conditions. The deconvoluted results from analyzing the raw data (Fig. 1A and B) are shown in Fig. 1C and D, respectively. A mass spectrum of the protein under denaturing acidic conditions showed only one predominant peak having a molecular mass of 14633 Da, which was almost identical to the theoretical molecular mass of mature LECT2 [2]. On the other hand, the spectrum of the protein under neutral conditions showed a significant signal of 14698 Da in addition to a major signal of 14633 Da that corresponded to the molecular weight revealed under acidic conditions. The mass difference of these two signals is 65 Da, which is almost identical to the atomic weight of zinc.

To confirm that the zinc atom is bound to LECT2, XAFS measurements were performed. Typical profiles of XAFS experiments are shown in Fig. 2. The XAFS profile of recombinant mouse LECT2 in Fig. 2A showed a *K* absorption edge of 1.2828 Å, indicating the protein contained a zinc atom [18]. A positive control experiment using the zinc-binding protein lysostaphin [19,20] is shown in Fig. 2B. The *K* absorption edge (1.2828 Å) wavelength indicating zinc absorption in lysostaphin was identical to that seen in the LECT2 XAFS data. These data indicate that recombinant mouse LECT2 contains a non-covalently bound zinc atom and strongly suggest that there is one zinc atom per molecule.

3.2. Oligomerization of mammalian LECT2 in vitro

The incubation experiments revealed that recombinant mammalian LECT2s oligomerize in vitro. Recombinant mouse LECT2

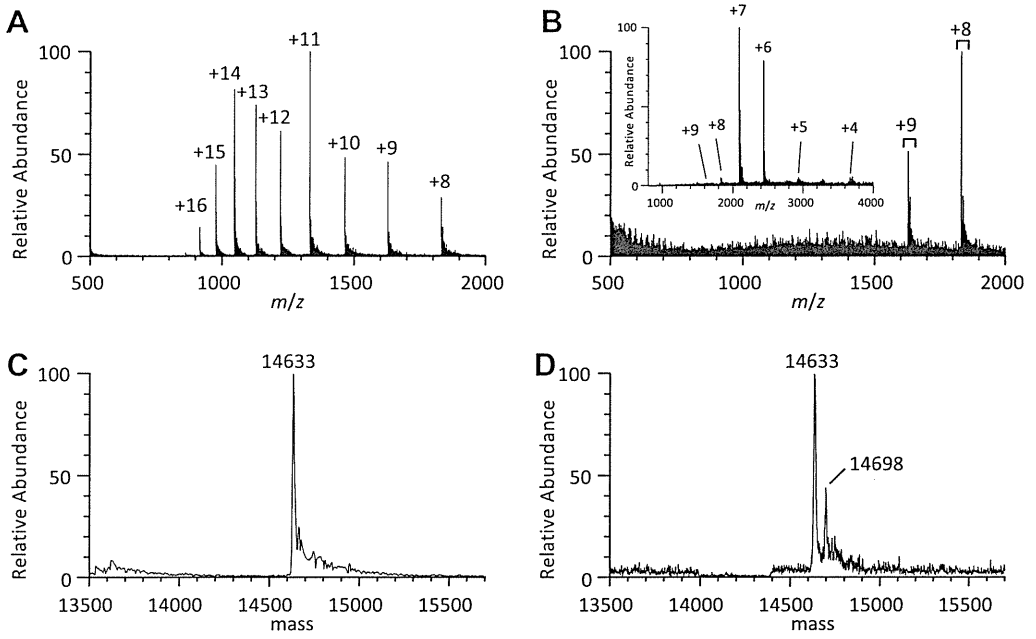

Fig. 1. Comparisons of electrospray ionization (ESI) mass spectra of mouse LECT2 under acidic (0.075% formic acid) and neutral (10 mM ammonium formate) conditions. Positive ion ESI mass spectra of LECT2 under acidic (A) and neutral (B) conditions. Charge states of LECT2 protein ions are indicated. The corresponding deconvoluted spectra of LECT2 under acidic (C) and neutral (D) conditions. The wider *m/z* range mass spectrum insets are shown in the upper left corner of the neutral conditions figure (B). Calculated molecular weights are indicated.

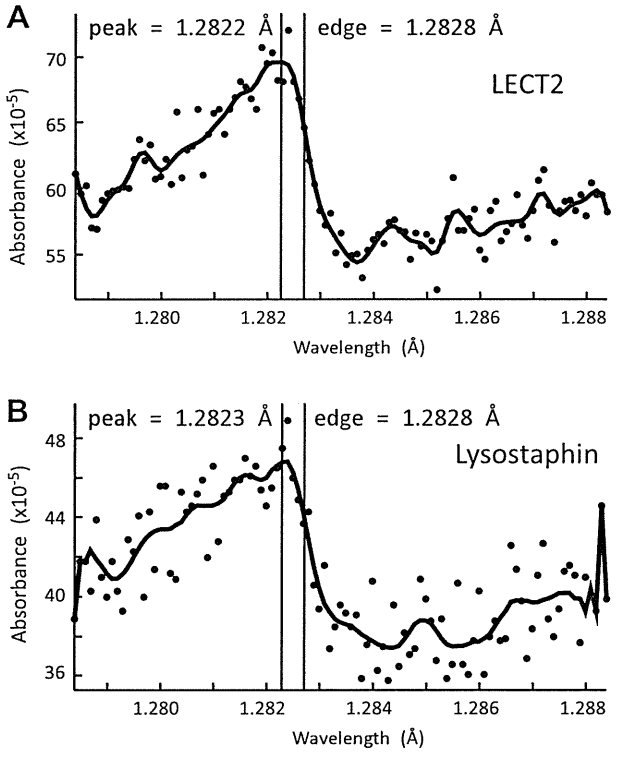

Fig. 2. A comparison of the fluorescence XAFS data at the Zn *K* absorption edge of LECT2 (A) and lysostaphin (B).

was incubated in buffer C (100 mM Tris–HCl pH 7.5, 150 mM NaCl) at 37 °C for one day. SDS–PAGE was then performed under non-reducing conditions, and LECT2 protein was detected by Western blotting using an anti-mouse LECT2 polyclonal antibody. Fig. 3A shows that the oligomerization occurred in a temperature-dependent manner. As shown in Supplemental Fig. 1, the oligomerization occurred in a time-dependent manner. SDS–PAGE carried out under reducing conditions showed a distinct pattern of oligomerization. Strangely, ladder bands migrating at 100–250 kDa and smear bands around the expected dimer position were detected in reduced SDS–PAGE. As shown in Supplemental Fig. 2, DTT treatment enhanced the oligomerization of LECT2 in a concentration-dependent manner. Furthermore, the intensity of the ladder bands migrating between 100 and 250 kDa increased over time in the experiments carried out at the high concentration of 200 mM DTT (Supplemental Fig. 3). Moreover, the state of the dimer in reduced SDS–PAGE was different from those observed in non-reduced SDS–PAGE. On the other hand, iodoacetate is known to be an alkylating agent, which irreversibly reacts with cysteine to block disulfide bond formation. As shown in Supplemental Fig. 4, iodoacetate treatment inhibited higher-order oligomerization except dimers and trimers. Strangely, the formation of lower-order oligomers increased at 10 mM of iodoacetate. The mechanism behind these oligomerization variations is not clear, but the disulfide bonds among LECT2s appeared to be involved in oligomer formation. As shown in Fig. 3A, oligomers of LECT2 were not detectable on a silver-stained gel following a 1-day incubation.

Oligomerization of recombinant human LECT2 produced by an animal cell line has also been observed, indicating that the oligomerization was not unique to mouse LECT2 (Fig. 3B).

3.3. Zinc suppresses oligomerization of mammalian LECT2

As shown in Fig. 4A, treatment with EDTA as a zinc ion chelator enhanced the oligomerization of LECT2, and Zn^{2+} reduced it as compared with an untreated control (lanes 2 and 4 vs. lane 1). EGTA treatment also enhanced the oligomerization of LECT2 to a similar extent (lane 3). Both Ca^{2+} and Mg^{2+} ions slightly inhibited the oligomerization (lanes 5 and 6), but that inhibition was much lower than that seen following Zn^{2+} treatment. Furthermore, the possibility that incorporation of the zinc ion was reversible in LECT2 was explored. As shown in Fig. 4B, LECT2 was treated with EDTA for 6 h, and then EDTA was removed by dialysis against

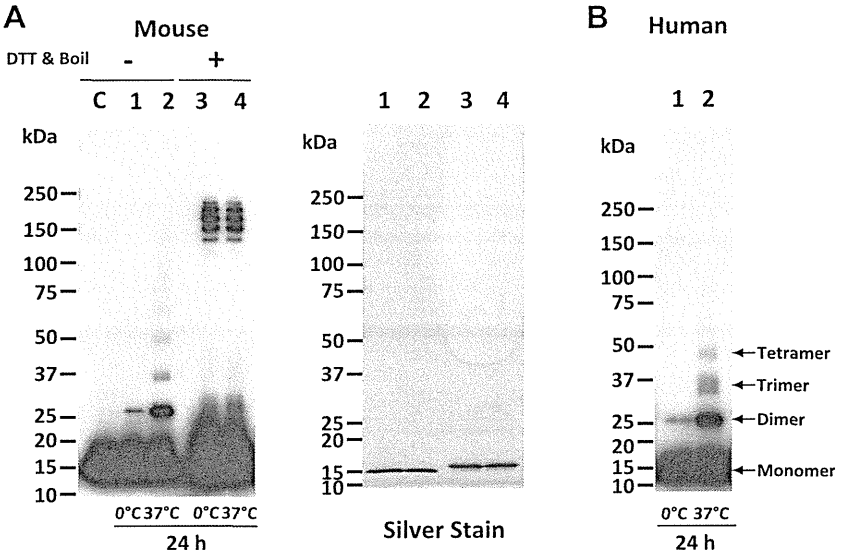

Fig. 3. Oligomerization assay of LECT2 in vitro. (A) Reaction solutions containing recombinant mouse LECT2 were incubated for 24 h at 0 °C (lanes 1 and 3) and 37 °C (lanes 2 and 4). Each reaction was divided into two aliquots, and the reactions were stopped by adding SDS–PAGE sample buffer without (lanes 1 and 2) or with (lanes 3 and 4) DTT (200 mM) and boiling (for 5 min). SDS–PAGE was then carried out on a 5–20% gradient polyacrylamide gel followed by Western blotting. A non-incubated sample was loaded in the first lane (C). Left image: Western blot. Right image: silver stained gel. (B) Recombinant human LECT2 was incubated for 24 h at 0 °C (lane 2) and 37 °C (lane 3).

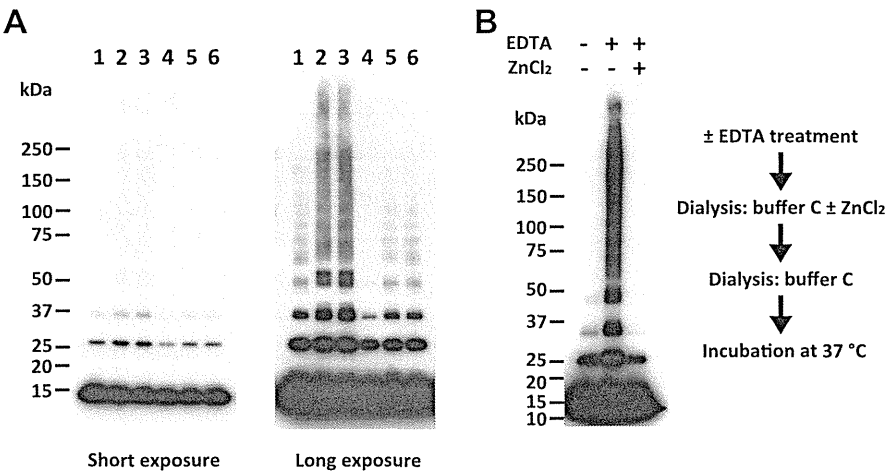

Fig. 4. Zinc inhibits the oligomerization of LECT2 in vitro. (A) The recombinant mouse LECT2 protein solution was incubated with chelators or divalent cations for 24 h 37 °C and then analyzed by SDS–PAGE and Western blotting. Lane: 1, control; 2, 5 mM EDTA; 3, 5 mM EGTA; 4, 5 mM $ZnCl_2$; 5, 5 mM $CaCl_2$; 6, 5 mM $MgCl_2$. Left image: short exposure of Western blot. Right image: long exposure of Western blot. (B) The effect of added zinc on EDTA-treated LECT2. Two aliquots of recombinant mouse LECT2 protein solution were incubated with 5 mM EDTA for 6 h at 4 °C and then dialyzed against buffer C (lane 2) or buffer C containing 5 mM $ZnCl_2$ and subsequently against buffer C to remove excess zinc ions (lane 3). In parallel, an aliquot of LECT2 solution as a control was incubated without EDTA for 6 h at 4 °C and then dialyzed against buffer C (lane 1). All dialyses were carried out at 4 °C. Following the final dialysis against fresh buffer C, all three samples were incubated for 24 h at 37 °C and then analyzed by SDS–PAGE and Western blotting.

buffer C with or without 5 mM $ZnCl_2$. Free zinc ions were subsequently removed by dialysis against buffer C. Consequently, oligomerization stimulated by EDTA treatment was suppressed to below the control level by introduction of zinc. Taken together, these results indicated that zinc contributed to the stabilization of the LECT2 structure and strongly suggested that incorporation of the zinc ion in LECT2 was reversible.

4. Discussion

Zinc is known to play a structural or catalytic role in many proteins [21]. The sequence homology of LECT2 with a zinc metalloprotease family suggested that zinc might stabilize the LECT2 structure. The effect of zinc on the oligomerization state of LECT2 was therefore examined. This report presents the results of ESI-MS and XAFS analyses, which demonstrate that LECT2 contains a non-covalently bound zinc atom. LECT2 is a member of the peptidase M23 family. The structures of four proteins in this family have been determined by X-ray crystallography (PDBj; http://www.pdbj.org). Three additional members of the M23B subfamily were identified by a homology search with LECT2, which contains two conserved motifs (HxxD and HxH) that were associated with zinc ion binding in these three proteins. Fig. 5 shows the corresponding amino acid sequence alignments. Each member of this family has one zinc ion per protein molecule. Together with ESI-MS data presented herein, this indicates that mammalian LECT2 also binds to one zinc ion per molecule.

Our results also demonstrate that mammalian LECT2 protein oligomerizes in vitro. Mammalian LECT2 has three disulfide bonds [3]. The oligomerization was strongly affected by DTT treatment, as

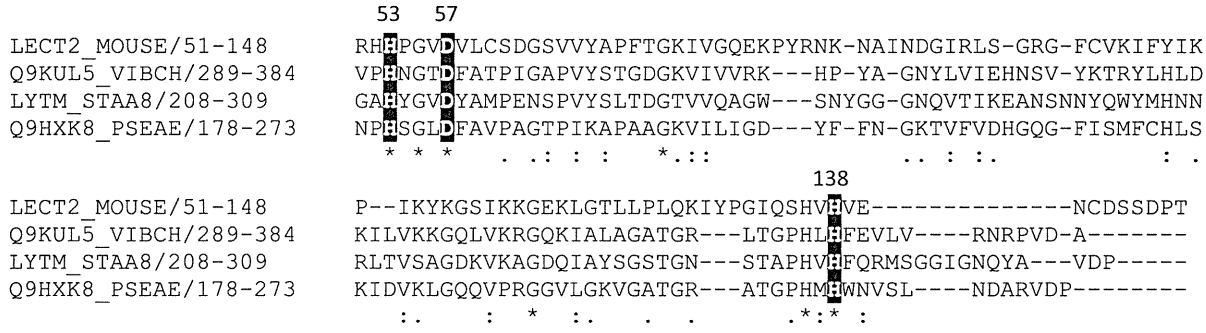

Fig. 5. Alignments of the zinc binding regions of mouse LECT2 and other peptidase M23B family proteins. Q9KUL5_VIBCH; Putative uncharacterized protein VC0503 from *Vibrio cholerae*, LYTM_STAA8; Glycyl-glycine endopeptidase LytM from *Staphylococcus aureus* strain NCTC 8325, Q9HXK8_PSEAE; Putative uncharacterized protein from *Pseudomonas aeruginosa*. Putative amino acid residues that directly bind to zinc are shown in black boxes.

shown in Fig. 3B and in Supplemental Figs. 2 and 3. Furthermore, the inhibition of higher-order oligomer formation by iodoacetate treatment as shown in Supplemental Fig. 4 also reflects the contribution of disulfide bonds. Dimer (occasionally trimer and tetramer) formation was found at low temperature and in the presence of zinc or iodoacetate. The kinetics of lower-order oligomer formation might be faster than that of higher-order oligomer formation. LECT2 might non-covalently form oligomers under physiological conditions. Actually, Mim-1, which is the chicken ortholog of LECT2, consists of two repeated units of LECT2 that associate to form a dimer [22]. Oligomers of LECT2 were not detectable on a silver-stained gel following a 1-day incubation (Fig. 3B). A faint band at the assumed positions for dimers was detected following a 7-day incubation, but further oligomerization of LECT2 over that incubation period was not observed (data not shown). Considering the sensitivity of the silver-stain, we estimate one or less percent of total LECT2 was involved in this reaction. The most likely explanation for this low reactivity is that the most of the cysteine residues in the recombinant LECT2 formed sulfide bonds. Therefore only a small number of residual cysteine residues that did not form the disulfide bonds were available to participate in this reaction. It is known that oligomerization of a recombinant protein is occasionally caused by oxidation [23,24]. On the other hand, it is possible that another structural property of LECT2 caused the oligomerization, as in the case of β_2-microglobulin [25].

LECT2 contains a zinc atom, and zinc ions inhibited the formation of oligomers, indicating that zinc stabilizes the LECT2 structure. ESI-MS analysis has also been used to monitor protein folding and protein complexes [26]. In comparing Fig. 1A and B, it appears that fewer accessible protonation sites would partially reflect a more compact LECT2 protein folding induced by zinc complex formation. It is possible that zinc plays a crucial role in LECT2 activity as well. For example, as LECT2 is a member of the M23 protease family, we are analyzing the possibility that it is a protease. Until now, we have not found any protease activities of LECT2 after testing it against many possible protein substrates (serum albumin, carbonic anhydrase, insulin-beta chain, aprotinin and ribonuclease A in bovine, rabbit myosin and phosphorylase b, hen egg ovalbumin and lysozyme, soybean trypsin inhibitor, glutathione S-transferase of *Schistosoma japonicum*, maltose binding protein and β-galactosidase of *Escherichia coli*; data not shown). Furthermore, we could not find any lysostaphin-like activity of LECT2 against *Staphylococcus aureus* (data not shown) [27]. If LECT2 has a protease activity, the substrate specificity might be strict. On the other hand, LECT2 might not have a protease activity similar to murein hydrolase activator NlpD protein, which also belongs to the M23 protease family [28].

Recently, it has been reported that LECT2 is a novel renal amyloid protein [10]. Although LECT2 amyloidosis has been recognized only recently, it does not appear to be a rare occurrence [11]. One feature of amyloid proteins is their beta-sheet rich structures. Actually, some amyloid proteins, such as immunoglobulin light chain, β_2-microglobulin and lysozyme, have extensive beta-sheet structure in their native state, and a beta-sheet may be stabilized by protein aggregation [29]. We have already indicated that LECT2 has several beta-sheets but no alpha-helix [30]. The oligomerization of LECT2 might offer a clue for further investigations of amyloid fibril formation, to further clarify the mechanism of LECT2 oligomerization.

Acknowledgments

We thank Drs. Yuuki Nakamura, Go Ueno, Takaaki Hikima and Masaki Yamamoto for help with XAFS analysis using the mail-in system in SPring-8. We also thank Akio Ebihara, Mayumi Kanagawa and Yoshiaki Kitamura for their help in data collection at the SPring-8 beamlines BL26B1 and BL26B2. Finally, we thank Drs. Koichi Tanabe and Keiko Ishino for useful discussions. This work was supported in part by Grants-in-Aid for Scientific Research from the Ministry of Education, Science, Sports and Technology of Japan (MEXT) to A. Okumura (21791422 and 24790938) and S. Yamagoe (23590275), and by the X-ray Free Electron Laser Utilization Research Project of MEXT to N. Dohmae.

Appendix A. Supplementary data

Supplementary data associated with this article can be found, in the online version, at http://dx.doi.org/10.1016/j.febslet.2013.01.025.

References

[1] Yamagoe, S., Yamakawa, Y., Matsuo, Y., Minowada, J., Mizuno, S. and Suzuki, K. (1996) Purification and primary amino acid sequence of a novel neutrophil chemotactic factor LECT2. Immunol. Lett. 52, 9–13.
[2] Yamagoe, S., Mizuno, S. and Suzuki, K. (1998) Molecular cloning of human and bovine LECT2 having a neutrophil chemotactic activity and its specific expression in the liver. Biochim. Biophys. Acta 1396, 105–113.
[3] Okumura, A., Suzuki, T., Dohmae, N., Okabe, T., Hashimoto, Y., Nakazato, K., Ohno, H., Miyazaki, Y. and Yamagoe, S. (2009) Identification and assignment of three disulfide bonds in mammalian leukocyte cell-derived chemotaxin 2 by matrix-assisted laser desorption/ionization time-of-flight mass spectrometry. Biosci. Trends 3, 139–143.
[4] Saito, T., Okumura, A., Watanabe, H., Asano, M., Ishida-Okawara, A., Sakagami, J., Sudo, K., Hatano-Yokoe, Y., Bezbradica, J.S., Joyce, S., Abo, T., Iwakura, Y., Suzuki, K. and Yamagoe, S. (2004) Increase in hepatic NKT cells in leukocyte cell-derived chemotaxin 2-deficient mice contributes to severe concanavalin A-induced hepatitis. J. Immunol. 173, 579–585.
[5] Okumua, A., Saito, T., Otani, I., Kojima, K., Yamada, Y., Ishida-Okawara, A., Nakazato, K., Asano, M., Kanayama, K., Iwakura, Y., Suzuki, K. and Yamagoe, S. (2008) Suppressive role of leukocyte cell-derived chemotaxin 2 in mouse anti-type II collagen antibody-induced arthritis. Arthritis Rheum. 58, 413–421.
[6] Phesse, T.J., Parry, L., Reed, K.R., Ewan, K.B., Dale, T.C., Sansom, O.J. and Clarke, A.R. (2008) Deficiency of Mbd2 attenuates Wnt signaling. Mol. Cell. Biol. 28, 6094–6103.

[7] Dang, M.H., Kato, H., Ueshiba, H., Omori-Miyake, M., Yamagoe, S., Ando, K., Imanishi, K., Arimura, Y., Haruta, I., Kotani, T., Ozaki, M., Suzuki, K., Uchiyama, T. and Yagi, J. (2010) Possible role of LECT2 as an intrinsic regulatory factor in SEA-induced toxicity in D-galactosamine-sensitized mice. Clin. Immunol. 137, 311–321.
[8] Ong, H.T., Tan, P.K., Wang, S.M., Hian Low, D.T., Ooi, L.L. and Hui, K.M. (2011) The tumor suppressor function of LECT2 in human hepatocellular carcinoma makes it a potential therapeutic target. Cancer Gene Ther. 18, 399–406.
[9] Anson, M., Crain-Denoyelle, A.M., Baud, V., Chereau, F., Gougelet, A., Terris, B., Yamagoe, S., Colnot, S., Viguier, M., Perret, C. and Couty, J.P. (2012) Oncogenic β-catenin triggers an inflammatory response that determines the aggressiveness of hepatocellular carcinoma in mice. J. Clin. Invest. 122, 586–599.
[10] Benson, M.D., James, S., Scott, K., Liepnieks, J.J. and Kluve-Beckerman, B. (2008) Leukocyte chemotactic factor 2: a novel renal amyloid protein. Kidney Int. 74, 218–222.
[11] Murphy, C.L., Wang, S., Kestler, D., Larsen, C., Benson, D., Weiss, D.T. and Solomon, A. (2010) Leukocyte chemotactic factor 2 (LECT2)-associated renal amyloidosis: a case series. Am. J. Kidney Dis. 56, 1100–1107.
[12] Yamagoe, S., Akasaka, T., Uchida, T., Hachiya, T., Okabe, T., Yamakawa, Y., Arai, T., Mizuno, S. and Suzuki, K. (1997) Expression of a neutrophil chemotactic protein LECT2 in human hepatocytes revealed by immunochemical studies using polyclonal and monoclonal antibodies to a recombinant LECT2. Biochem. Biophys. Res. Commun. 237, 116–120.
[13] Okazaki, N., Hasegawa, K., Ueno, G., Murakami, H., Kumasaka, T. and Yamamoto, M. (2008) Mail-in data collection at SPring-8 protein crystallography beamlines. J. Synchrotron Radiat. 15, 288–291.
[14] Ueno, G., Hirose, R., Ida, K., Kumasaka, T. and Yamamoto, M. (2004) Sample management system for a vast amount of frozen crystals at SPring-8. J. Appl. Crystallogr. 37, 867–873.
[15] Ueno, G., Kanda, H., Kumasaka, T. and Yamamoto, M. (2005) Beamline Scheduling Software: administration software for automatic operation of the RIKEN structural genomics beamlines at SPring-8. J. Synchrotron Radiat. 12, 380–384.
[16] Ueno, G., Kanda, H., Hirose, R., Ida, K., Kumasaka, T. and Yamamoto, M. (2006) RIKEN structural genomics beamlines at the SPring-8; high throughput protein crystallography with automated beamline operation. J. Struct. Funct. Genomics 7, 15–22.
[17] Loo, J.A. (1997) Studying noncovalent protein complexes by electrospray ionization mass spectrometry. Mass Spectrom. Rev. 16, 1–23.
[18] Sasaki, S. (1989) Numerical tables of anomalous scattering factors calculated by the Cromer and Liberman's method. KEK Report 14–88, 1–136.
[19] Trayer, H.R. and Buckley III, C.E. (1970) Molecular properties of lysostaphin, a bacteriolytic agent specific for *Staphylococcus aureus*. J. Biol. Chem. 245, 4842–4846.
[20] Odintsov, S.G., Sabala, I., Marcyjaniak, M. and Bochtler, M. (2004) Latent LytM at 1.3 Å resolution. J. Mol. Biol. 335, 775–785.
[21] Lee, Y.M. and Lim, C. (2008) Physical basis of structural and catalytic Zn-binding sites in proteins. J. Mol. Biol. 379, 545–553.
[22] Ness, S.A., Marknell, A. and Graf, T. (1989) The v-*myb* oncogene product binds to and activates the promyelocyte-specific *mim-1* gene. Cell 59, 1115–1125.
[23] Yamamoto, Y., Kato, Z., Matsukuma, E., Li, A., Omoya, K., Hashimoto, K., Ohnishi, H. and Kondo, N. (2004) Generation of highly stable IL-18 based on a ligand–receptor complex structure. Biochem. Biophys. Res. Commun. 317, 181–186.
[24] Seno, M., Sasada, R., Iwane, M., Sudo, K., Kurokawa, T., Ito, K. and Igarashi, K. (1988) Stabilizing basic fibroblast growth factor using protein engineering. Biochem. Biophys. Res. Commun. 151, 701–708.
[25] Liu, C., Sawaya, M.R. and Eisenberg, D. (2011) β_2-microglobulin forms three-dimensional domain-swapped amyloid fibrils with disulfide linkages. Nat. Struct. Mol. Biol. 18, 49–55.
[26] Winston, R.L. and Fitzgerald, M.C. (1997) Mass spectrometry as a readout of protein structure and function. Mass Spectrom. Rev. 16, 165–179.
[27] DeHart, H.P., Heath, H.E., Heath, L.S., LeBlanc, P.A. and Sloan, G.L. (1995) The lysostaphin endopeptidase resistance gene (*epr*) specifies modification of peptidoglycan cross bridges in *Staphylococcus simulans* and *Staphylococcus aureus*. Appl. Environ. Microbiol. 61, 1475–1479.
[28] Uehara, T., Parzych, K.R., Dinh, T. and Bernhardt, T.G. (2010) Daughter cell separation is controlled by cytokinetic ring-activated cell wall hydrolysis. EMBO J. 29, 1412–1422.
[29] Soto, C. (2001) Protein misfolding and disease; protein refolding and therapy. FEBS Lett. 498, 204–207.
[30] Ito, M., Nagata, K., Yumoto, F., Yamagoe, S., Suzuki, K., Adachi, K. and Tanokura, M. (2004) ^{1}H, ^{13}C, ^{15}N resonance assignments of the cytokine LECT2. J. Biomol. NMR 29, 543–544.

Diabetol Int (2011) 2:160–161
DOI 10.1007/s13340-011-0053-8

COMMENTARY

Role of the podocyte signal-transduction systems in the pathogenesis of diabetic nephropathy

Yasushi Kaburagi · Hiroyuki Unoki-Kubota

Received: 19 October 2011 / Published online: 12 November 2011

Diabetic nephropathy, which develops in 30–40% of diabetic patients, is a leading cause of end-stage renal disease (ESRD), accounting for more than 40% of new ESRD cases undergoing treatment in the USA and other developed countries [1, 2]. In its initial stage, diabetic patients excrete macromolecules such as albumin, indicating an abnormality in the glomerular permeability barrier, followed by a gradual decline of GFR with the appearance of overt proteinuria [3]. The glomerular permeability barrier consists of endothelial cells, the glomerular basement membrane, and podocytes. Podocytes are highly specialized epithelial cells with interdigitating foot processes that participate in the prevention of proteinuria [4]. In the early stage of diabetic nephropathy, effacement of the foot processes is observed in podocytes, resulting in the leakage of macromolecules, including albumin, into the urine [4]. Loss of trace amounts of albumin in the urine, microalbuminuria, has been regarded as an early marker of diabetic nephropathy, although microalbuminuria is also observed in patients with metabolic syndrome, indicating that insulin resistance may cause podocyte injury [5].

To examine the role of podocyte insulin signaling in the pathogenesis of diabetic nephropathy, Welsh et al. [6] recently analyzed mice with podocyte-specific deletion of the insulin receptor. They showed that these mice developed significant proteinuria by 5 weeks of age; histological glomerular changes resembling those of diabetic nephropathy, for example effacement of podocyte foot processes, thickening of the basement membrane, accumulation of mesangial matrix, and glomerulosclerosis in a normoglycemic environment, were also observed. In in-vivo and in-vitro analysis of podocytes lacking the insulin receptor, both the mitogen-activated protein kinase (MAPK) and phosphatidylinositol 3-kinase/Akt pathways, the two major pathways downstream of the insulin receptor, were shown to be abrogated. It was also reported that insulin-induced reorganization of actin cytoskeleton in podocytes, which, in investigations of familial nephritic syndromes, was revealed to be important in the maintenance of the glomerular permeability barrier [7], was affected by the absence of the insulin receptor. These findings suggested that impaired insulin signaling in podocytes is sufficient for development of some pathological features of diabetic nephropathy, although its molecular mechanism was not fully investigated. In addition, in these mice, the role of other insulin-regulated pathways important for the maintenance of podocyte function, such as autophagy and mammalian target of rapamycin (mTOR) pathways were not evaluated [8, 9].

Autophagy is a biological process that plays a crucial role in maintaining cell integrity by degradation and recycling of cytosolic proteins and organelles [8]. As podocytes are terminally differentiated postmitotic cells, autophagy is critically important for maintenance of cellular homeostasis. In fact, podocyte-specific deletion of autophagy-related 5 (Atg5), a key regulator of the autophagic process, led to a glomerulopathy in aging mice that was accompanied by accumulation of oxidized and ubiquitinated proteins, ER stress, and proteinuria [10]. This autophagic pathway is inhibited by insulin, and by other growth factors and nutrients, for example

Y. Kaburagi (✉) · H. Unoki-Kubota
Department of Diabetic Complications,
Diabetes Research Center, Research Institute,
National Center for Global Health and Medicine,
1-21-1 Toyama, Shinjuku-ku, Tokyo 162-8655, Japan
e-mail: kaburagi@ri.ncgm.go.jp

glucose and amino acids, via a rapamycin-sensitive protein complex, termed mTOR complex 1 (mTORC1), containing an evolutionarily conserved serine/threonine protein kinase, mTOR [9]. Animal studies have revealed that experimental inhibition of mTORC1 activity upregulated in diabetic state via rapamycin has a beneficial effect on the treatment of diabetic nephropathy [11]. According to these findings, Inoki et al. [12] recently generated mice with podocyte-specific ablation of an upstream negative regulator of mTORC1, TSC1, to analyze the effects of constitutive mTORC1 activation on glomerular function. Podocyte-specific mTORC1 activation caused thickening of the glomerular basement membrane, proteinuria, and mesangial expansion, in addition to podocyte loss. These diabetic nephropathy-like features were ameliorated by rapamycin treatment or genetic suppression of mTORC1 activity by podocyte-specific knockout of Raptor, an essential component of mTORC1 [12]. Conversely, Gödel [13] analyzed mice lacking podocyte mTORC1 activity by podocyte-specific knockout of Raptor, and demonstrated that loss of podocyte mTORC1 activity also caused albuminuria and progressive glomerulosclerosis. They also showed that additional loss of podocyte mTORC2 activity by podocyte-specific knockout of Rictor, an essential component of mTORC2, aggravated the glomerular lesions, indicating that both of the two mTOR complexes are involved in the maintenance of podocyte function [13]. These studies convincingly showed that podocyte mTOR activity is essential to the maintenance of glomerular function, although the extent to which these mTOR pathways are involved in the pathogenesis of nephropathy in diabetic patients remains unclear. Moreover, taking into account that patients with tuberous sclerosis caused by TSC1 or TSC2 mutations do not develop glomerular lesions resembling those of diabetic nephropathy [14], these findings in animal models should be cautiously examined for future clinical applications in the treatment of diabetic nephropathy.

Collectively, recent animal studies manipulating podocyte insulin-regulated signal transduction have verified that perturbation of this system in podocytes is sufficient to cause development of pathological changes similar to those of diabetic nephropathy. Further investigation is needed to clarify the molecular mechanisms of human diabetic nephropathy.

References

1. Stewart JH, McCredie MR, Williams SM, Jager KJ, Trpeski L, McDonald SP. ESRD Incidence Study Group. Trends in incidence of treated end-stage renal disease, overall and by primary renal disease, in persons aged 20–64 years in Europe, Canada and the Asia-Pacific region, 1998–2002. Nephrology. 2007;12:520–7.
2. Centers for Disease Control, Prevention (CDC). Racial differences in trends of end-stage renal disease, by primary diagnosis–United States, 1994–2004. MMWR Morb Mortal Wkly Rep. 2007;56:253–6.
3. Fioretto P, Mauer M. Histopathology of diabetic nephropathy. Semin Nephrol. 2007;27:195–207.
4. Stieger N, Worthmann K, Schiffer M. The role of metabolic and haemodynamic factors in podocyte injury in diabetes. Diabetes Metab Res Rev. 2011;27:207–15.
5. Ninomiya T, Kiyohara Y. Albuminuria and chronic kidney disease in association with the metabolic syndrome. J Cardiometab Syndr. 2007;2:104–7.
6. Welsh GI, Hale LJ, Eremina V, Jeansson M, Maezawa Y, Lennon R, Pons DA, Owen RJ, Satchell SC, Miles MJ, Caunt CJ, McArdle CA, Pavenstädt H, Tavaré JM, Herzenberg AM, Kahn CR, Mathieson PW, Quaggin SE, Saleem MA, Coward RJ. Insulin signaling to the glomerular podocyte is critical for normal kidney function. Cell Metab. 2010;12:329–40.
7. Zenker M, Machuca E, Antignac C. Genetics of nephrotic syndrome: new insights into molecules acting at the glomerular filtration barrier. J Mol Med. 2009;87:849–57.
8. Weide T, Huber TB. Implications of autophagy for glomerular aging and disease. Cell Tissue Res. 2011;343:467–73.
9. Wullschleger S, Loewith R, Hall MN. TOR signaling in growth and metabolism. Cell. 2006;124:471–84.
10. Hartleben B, Gödel M, Meyer-Schwesinger C, Liu S, Ulrich T, Köbler S, Wiech T, Grahammer F, Arnold SJ, Lindenmeyer MT, Cohen CD, Pavenstädt H, Kerjaschki D, Mizushima N, Shaw AS, Walz G, Huber TB. Autophagy influences glomerular disease susceptibility and maintains podocyte homeostasis in aging mice. J Clin Invest. 2010;120:1084–96.
11. Huber TB, Walz G, Kuehn EW. mTOR and rapamycin in the kidney: signaling and therapeutic implications beyond immunosuppression. Kid Int. 2011;79:502–11.
12. Inoki K, Mori H, Wang J, Suzuki T, Hong S, Yoshida S, Blattner SM, Ikenoue T, Rüegg MA, Hall MN, Kwiatkowski DJ, Rastaldi MP, Huber TB, Kretzler M, Holzman LB, Wiggins RC, Guan KL. mTORC1 activation in podocytes is a critical step in the development of diabetic nephropathy in mice. J Clin Invest. 2011;121:2181–96.
13. Gödel M, Hartleben B, Herbach N, Liu S, Zschiedrich S, Lu S, Debreczeni-Mór A, Lindenmeyer MT, Rastaldi MP, Hartleben G, Wiech T, Fornoni A, Nelson RG, Kretzler M, Wanke R, Pavenstädt H, Kerjaschki D, Cohen CD, Hall MN, Rüegg MA, Inoki K, Walz G, Huber TB. Role of mTOR in podocyte function and diabetic nephropathy in humans and mice. J Clin Invest. 2011;121:2197–209.
14. Siroky BJ, Yin H, Bissler JJ. Clinical and molecular insights into tuberous sclerosis complex renal disease. Pediatr Nephrol. 2011;26:839–52.

Diabetes Frontier

別刷

メディカルレビュー社

〒541-0045 大阪市中央区道修町1-5-18 朝日生命道修町ビル　TEL 06-6223-1469 FAX 06-6223-1245

Ⅱ　プロテオミクス

プロテオミクスを用いた糖尿病診断マーカーの探索

国立国際医療研究センター研究所 糖尿病研究センター 臓器障害研究部
鏑木　康志
Yasushi Kaburagi

Key Words
糖尿病
細小血管症
プロテオミクス
バイオマーカー
質量分析

はじめに

糖尿病は国内外で急増しており，国際糖尿病連合（IDF）の2010年の発表によると世界の糖尿病有病数は2億8,500万人と全人口の6.4％を占めている。また，世界の糖尿病患者は2030年には2010年の50％以上増の4億3,800万人と推計されており，発展途上国を含む全世界で脅威になっている。日本においても近年糖尿病を含む生活習慣病は急増しており，厚生労働省の2007年国民健康・栄養調査では糖尿病有病者は890万人と5年前の調査と比較して20％以上も増加しており，また糖尿病予備軍［HbA1c（JDS値）5.6％以上］を含めると2,210万人と5年前との比較では30％以上の増加となっている。さらに，糖尿病罹患者では腎症，網膜症，神経障害といった糖尿病に固有な細小血管症が出現し，2009年の統計では糖尿病性腎症が原因の透析導入患者数は年間約1万6,400人と透析導入原因疾患の44.5％を占め，糖尿病網膜症からの失明患者は年間3,000人と失明原因の2位，糖尿病性壊疽による下肢切断の原因となる糖尿病性神経障害も糖尿病患者の1/3以上と，糖尿病性合併症による健康障害は国民健康上大きな問題になっている。これらの合併症は進行するまで自覚症状を伴わないため，糖尿病合併症の病期や予後・進行性などを的確かつ簡便に診断可能な診断指標（バイオマーカー）が開発されれば，糖尿病合併症の予防，早期治療に有用であり，その意義は高い。本稿では，プロテオミクスの手法を用いた糖尿病診断マーカー，特に糖尿病合併症マーカーの探索研究の現状および今後の方向性について概説する。

Ⅰ　糖尿病とバイオマーカー

バイオマーカーとは尿や血清などの生体試料中にある物質で，生体内の生物学的あるいは病理学的プロセスを定量

的に評価可能な指標である。また，疾患治療におけるエンドポイントである患者の死亡，疾患によるイベントなどの発生可能なバイオマーカーはサロゲート(代用)マーカーと呼ばれ，有用なサロゲートマーカーを用いれば臨床試験にかかる時間および費用を節約することが可能となるため，その開発には大きな意義がある[1)2)]。

糖尿病の診療においては，血糖，HbA1cが血糖コントロールの指標となるバイオマーカーとして広く用いられている。これらのバイオマーカーと糖尿病性細小血管症の関連性については，過去の多くの大規模臨床研究によって糖尿病合併症の発症および進行が長期の血糖コントロールと強い関連性があることはすでに明らかになっている[3)4)]。ところが，個々の患者において糖尿病合併症の有無あるいは進行するか否かを予測可能な血清あるいは尿マーカーは現時点では存在しない。たとえば，糖尿病性腎症では微量アルブミン尿が腎症の病期判定に使われており，微量アルブミン尿を呈する場合は腎症第2期と診断される。ところが，1型および2型糖尿病のいずれにおいても6年間の追跡調査の結果では，微量アルブミン尿から正常化する患者が40～50％を占めており，微量アルブミン尿は糖尿病性腎症のサロゲートエンドポイントとはなりえない[5)6)]。

Ⅱ　糖尿病合併症の組織サンプルでのプロテオーム解析

このため，糖尿病合併症の診断マーカーとなりうる蛋白をプロテオーム解析の手法を用いて探索することは有意義であると考えられる。そのためには，まず合併症の場となる組織(腎臓，網膜，神経，血管など)がプロテオーム解析の対象となる。たとえば，糖尿病性腎症については新潟大学のYoshidaらが，手術時に摘出した腎臓をミンチした後にふるい操作にかけて糸球体を単離し，SDS-PAGE後に切り出したバンドから高速液体クロマトグラフ質量分析計(LC-MS)にて解析し，2966遺伝子に由来する6,686個の蛋白を同定している[7)]。また，この研究グループは腎生検の組織切片からlaser microdisectionにより糸球体を採取し，高感度の二次元電気泳動法により糸球体由来蛋白の定量解析を可能とする実験系を確立している[8)]。これらの解析が糖尿病性腎症の診断あるいは治療に有用な蛋白の発見につながる可能性がある。

また，糖尿病網膜症については，患者からの合併症の場となる網膜の採取が不可能なため，増殖網膜症に対する硝子体手術時に採取される硝子体を用いたプロテオーム解析が行われている[9)-11)]。最近の分析結果では，電気泳動あるいは多次元クロマトグラフィにて分画したサンプルをLC-MSにて解析することによって，500個程度の蛋白が増殖生網膜症の硝子体サンプルから同定されており[10)]，これらの蛋白から増殖網膜症の新しい診断法が確立されることが期待される。

Ⅲ　糖尿病合併症の血清・血漿のプロテオーム解析の問題点およびその克服のためのアプローチ

血液は糖尿病診療の現場で日常的に採取されるため，血清・血漿はバイオマーカー探索のための第一の研究対象となる。ところが，糖尿病は全身疾患であるため，同定された血清蛋白の変動がどの臓器あるいは組織のどのような病態に起因するかを特定するのは困難である。また，糖尿病では比較的早期から動脈硬化が起こり，特に糖尿病性腎症を合併した糖尿病患者では腎症の進行に伴って心血管疾患による死亡率が高まることが報告されている[12)]。このため，単純に糖尿病性腎症患者の血液サンプルからプロテオーム解析を行っても，腎症の指標となる血液マーカーを発見するのは困難である[13)-15)]。

近年，あらかじめ判明しているバイオマーカー候補蛋白について質量分析器を用いて高感度で特異的に定量できるselected reaction monitoring(SRM)/multiple reaction monitoring(MRM)法による解析が使われるようになってきた[16)17)]。このSRM/MRM法の原理は図1に示すように，測定対象の蛋白試料をトリプシン消化して，液体クロマトグラフィにオンラインで接続した三連四十極型質量分析器(triple quadrupole mass spectrometer)で分析する。ペプチドを順次イオン化させて，Q1にて特定の質量をもつ親イオンのみを通過させ，選択した親イオンをQ2で限定的に破壊して断片化させて娘イオンを作り，Q3で断片化された特定の質量の娘イオンを定量する。定量する蛋白のQ1とQ3の2回の質量フィルターによって，非常に高いS/N比で選択性高く測定すること

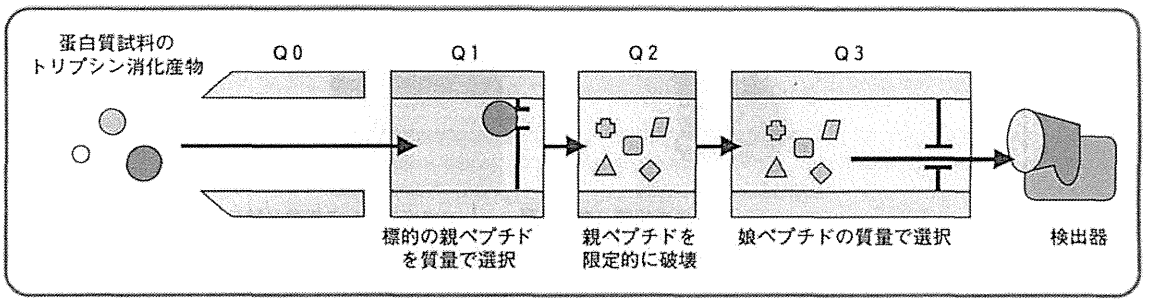

図1．MRM測定の原理

が可能である。本法を用いて糖尿病患者検体にて解析した研究はまだわずかだが，Kimらは糖尿病網膜症患者の硝子体サンプルにて有意に変動した12個の蛋白について，患者血漿にてSRM/MRM法にて定量している[18]。このSRM/MRM法を用いたアプローチでは，糖尿病患者の組織検体，疾患モデル動物，あるいは培養細胞にて糖尿病合併症との関連性が，前もって検証済みのバイオマーカー候補蛋白を糖尿病患者由来検体にて定量評価することが可能であるため，患者血清・血漿を網羅的に解析する場合と比較して，糖尿病合併症マーカーの探索および検証が効率化されることが期待される。

また，SRM/MRM法のもう1つの利点として，一度に多数のダブルフィルターを組むことができるので，血清・血漿のような複雑なサンプルであっても，一度に多数の蛋白の定量解析を行うこと可能である。近年，種々の疾患において単一のバイオマーカーによる病態把握には限界があるため，いくつものバイオマーカーを組み合わせたマルチマーカーの使用が提唱されている[19]。一斉分析が可能なMRM法は，この点でも大きく力を発揮する可能性がある。

Ⅳ　糖尿病患者尿のプロテオーム／ペプチドーム解析

尿蛋白の約70％が腎臓あるいは尿路に由来するとされている[20]。このため，腎臓における障害は尿中の蛋白あるいはペプチドのプロファイルに影響を与えると考えられ，尿のプロテオームあるいはペプチドーム解析は腎症マーカー探索の有力な手段となっている。数年前までは，二次元電気泳動に質量分析を組み合わせた解析法が尿プロテオーム解析の主要な手段であったが，二次元ゲル上で解析可能な蛋白スポットは数100に過ぎず，また解析に多大な労力および時間がかかる短所があった[20][21]。近年，よりハイスループットに蛋白の同定および定量を行うシステムとして，尿蛋白のトリプシン消化物を液体クロマトグラフィに直結した質量分析計（LC-MS）が用いられており，尿サンプルから2,000個以上の蛋白の同定が可能となっている[22]。また，トリプシン消化を行わなくても10kDa以下のペプチドはキャピラリー電気泳動装置あるいは液体クロマトグラフィに質量分析計を組み合わせたシステム（CE-MSまたはLC-MS）にて解析可能であり，Merchantらの報告[23]では，1型糖尿病患者で早期の腎機能障害で低下する尿中の3個のペプチドを見い出している。最近，多施設共同研究[24]にてCE-MSやLC-MSにて同定される尿ペプチド約5,000個がデータベース化されており，糖尿病を含めて尿ペプチドマーカー探索のための研究環境が整ってきている。

おわりに

本稿では，プロテオーム／ペプチドームの分野での糖尿病バイオマーカー探索研究の現状について概説した。筆者の所属する国立国際医療研究センターでは，厚生労働省の指導の下で行われている「創薬バイオマーカー探索研究」の一環として，糖尿病性細小血管症早期診断のための診断マーカー開発を目的とした研究が進行中である（図2）。本計画では，糖尿病患者から血清および尿を採取する際に，糖尿病性細小血管症および動脈硬化の進行度を含む詳細な